Lehigh University
Lehigh Preserve

Fritz Laboratory Reports | Civil and Environmental Engineering

1973

A galerkin method to evaluate three dimensional stress distributions and stress intensity factors in elastic bodies, Ph. D. dissertation 1973

Robert Jaccard

Follow this and additional works at: http://preserve.lehigh.edu/engr-civil-environmental-fritz-lab-reports

Recommended Citation
Jaccard, Robert, "A galerkin method to evaluate three dimensional stress distributions and stress intensity factors in elastic bodies, Ph. D. dissertation 1973" (1973). *Fritz Laboratory Reports.* Paper 418.
http://preserve.lehigh.edu/engr-civil-environmental-fritz-lab-reports/418

This Technical Report is brought to you for free and open access by the Civil and Environmental Engineering at Lehigh Preserve. It has been accepted for inclusion in Fritz Laboratory Reports by an authorized administrator of Lehigh Preserve. For more information, please contact preserve@lehigh.edu.

A GALERKIN METHOD TO EVALUATE THREE DIMENSIONAL STRESS DISTRIBUTIONS AND STRESS INTENSITY FACTORS IN ELASTIC BODIES

by

Robert Jaccard

FRITZ ENGINEERING
LABORATORY LIBRARY

A Dissertation
presented to the graduate committee
of Lehigh University
in candidacy for the Degree of
Doctor of Philosophy
in
Civil Engineering

Lehigh University
1973

CERTIFICATE OF APPROVAL

Approved and recommended for acceptance as a dissertation in partial fulfillment of the requirements of the degree of Doctor of Philosophy.

2/7/73
(Date)

John W. Fisher
Professor in Charge

Accepted 2/19/73
(Date)

Special Committee directing the doctoral work of Mr. Robert Jaccard

W. F. Chen
Professor W. Chen
Chairman

Professor B. T. Yen

G. R. Irwin
Professor G. R. Irwin

Professor D. A. VanHorn

ACKNOWLEDGMENTS

This analytical study was conducted at Fritz Engineering Laboratory, Lehigh University, Bethlehem, Pennsylvania. Dr. Lynn S. Beedle is Director of Fritz Engineering Laboratory and Dr. David A. VanHorn is Chairman of the Civil Engineering Department. The work was part of a low-cycle fatigue research program sponsored by the Office of Naval Research, Department of Defense under contract N00014-68-A-514; NR 064-509. The program manager for the overall research project is Dr. Lambert Tall.

The author is very grateful for the guidance and continuous encouragement of his supervisor Professor John W. Fisher. He also acknowledges the assistance and advice of Dr. S. Desai who has assisted with the computer program and offered many essential suggestions during the course of this study.

Thanks are also due to the members of the committee consisting of: Professors W. Chen, B. T. Yen, G. R. Irwin and D. A. VanHorn.

Acknowledgments are also due to Misses Phyllis Raudenbush and Karen Philbin for their care in typing the manuscript and to the staff of the drafting room for preparing the drawings.

TABLE OF CONTENTS

LIST OF TABLES

LIST OF FIGURES

ABSTRACT

In this dissertation a Galerkin method was developed to analyze elastic three dimensional boundary stress problems.

The method was developed in an attempt to evaluate the stress intensity factors for structural details. A set of stress functions, which satisfies equilibrium and compatibility throughout an elastic three dimensional body were used with an exterior Galerkin method. The parameters of the stress functions were computed, using the orthogonalization process of the Galerkin method. These parameters were determined so that the boundary stress conditions, including the crack surfaces, were satisfied in the mean. It is also demonstrated that the least square method is identical to the Galerkin method for boundary stress problems. Thus the method of least squares can be applied as well.

In this study three types of stress functions were used. These included polynomial stress functions, a closed form solution from the classical theory of elasticity and singular stress functions from fracture mechanics. A compatibility transformation for polynominal stress functions, which satisfy equilibrium was also developed.

The Galerkin method was applied first to a simple hexahedron with one embedded elliptical crack. Compatible polynomial stress functions up to power 4 and one singular stress function were used to obtain the stress intensity factors. The singular stress function described the three dimensional stress field around the elliptical crack in an elastic infinite body, assuming uniform pressure was acting on the crack surfaces. The solution obtained by the analysis showed that the plane strain condition assumed by Irwin for an embedded elliptical crack was reasonable. The inverse square root singularity of such singular stress functions was also demonstrated.

The method was then applied to more complex geometric details. This included a cruciform, a cover-plated beam flange and web and a hexahedron with a cylindrical hole. Up to fourth order power polynomial stress functions were used in an attempt to approximate the three dimensional stress fields in these complex structural details.

From this study it was concluded that polynomial stress functions are in general too smooth to describe the locally distributed stress fields in complex structural details.

Satisfactory results were only obtained when the method was applied to simple bodies such as the hexahedron where special stress functions could be used to reduce the error on the boundaries of the solids with finite dimensions.

These special stress functions define the local stress field, that exists near discontinuities in an infinite elastic solid. Depending on the problem and the geometry of the solid, they are either singular stress functions from fracture mechanics or closed form solutions from the classical theory of elasticity.

Available solutions of three dimensional solids with cracks have generally utilized an iterative method to develop the stress field and stress intensity factors. The Galerkin method used in this study does not require an iterative solution. The method utilizes a system of simultaneous equations to determine the stress-function parameters. The solution takes into account the stresses described by polynomial and special stress functions. It minimizes the residual stresses on the crack and boundary surfaces of the body so that these residuals are nearly zero or equal to the applied boundary stresses. The stress function parameters can be directly used to determine the stress field.

1. INTRODUCTION

In the last decade a large number of fatigue studies were done in various fields such as Aerospace, Mechanics and Civil Engineering.[1,2,3] These studies have indicated that fatigue cracks generally initiate and grow at discontinuities and changes in geometry. The data obtained in these tests have been evaluated by various methods including linear fracture mechanic concepts which has indicated that the methods can be successfully used to model the fatigue behavior of metallic structures.

The most popular basic model utilizes the correlation between crack growth rate and stress intensity range in the form of a power law:

$$\frac{da}{dN} = C \cdot \Delta K^n \qquad (1)$$

C and n are material constants that are experimentally determined from special crack growth specimens. For structural steels the values of these constants have been determined by a number of studies.[2] Tests on a larger number of welded details have indicated that the relationship.[4]

$$\frac{da}{dN} = 2 \times 10^{-10} \Delta K^3 \qquad (2)$$

where ΔK has units of ksi $\sqrt{in}$ and c has units of

$(ksi)^3\sqrt{in}$ cycles provides a reasonable explanation of the crack growth behavior of structural steels. It is apparent from Eq. 2 that the accuracy of the stress intensity range, ΔK, is most important for a reliable prediction of the fatigue life.

Many of welded details examined in Refs. 3 have indicated that the part-through crack was the most common type of crack to grow in structural joints.

G. R. Irwin[5] has reviewed the state of the art of semi-elliptical part-through crack research, stressing the fundamental aspects of the characterization of stresses near the crack border.

Various solutions for elastic stress intensity factors for semi-elliptical cracks are available. Yet there exist uncertainties as how to analyze the effects of complex geometries and stress fields. Other uncertainties have been noted by Little and Bunting,[6] such as plasticity effects, variable amplitude random loadings, etc. These will not be considered in the scope of this dissertation.

For infinite elastic bodies and plates with constant thickness, closed form solutions are available for the stress intensity factors for elliptical cracks.[8,9,10]

These solutions can be used for estimates in cases of finite geometries, if the crack size is small, compared to the specimen geometry (e.g. radius of hole, thickness of plate, etc.). The effect of the geometry is taken into account, using the local stress as the stress argument. This method is limited in its application. The zone of influence is not defined and the influence of the stress concentration factor with increasing crack size is not known. An approximation was successfully used by a number of investigators[10,11] to describe the stress intensity condition at fillet weld toes where the initial crack sizes are always small. Since most of the fatigue life is consumed while the crack is still relatively small this approach is justified.

Attempts have also been made to compute stress intensity factors for three dimensional problems. Marcal and Bettis[12] have reported an elastic-plastic solution for mode one using finite elements.

Smith[13] developed an iterative procedure using the classical solution of a semi circular crack in a semi-infinite elastic solid. Love's stress function was used to remove successively the stresses on the free surfaces and the crack surfaces. The inverse square root singularity at the leading edge of the crack was preserved. Shah et al.[14] replaced the semi-circular crack in Smith's solution with an elliptical one.

In this dissertation a numerical procedure is described, which permits all three stress-intensity factors to be determined in structural details.

A Galerkin approach is used to determine the parameters of three dimensional stress-functions. These parameters are unknowns to a set of linear simultaneous equations. They are determined so that the boundary stress conditions, including the crack surfaces, are satisfied in the mean and the error is minimized in some sense.

It is demonstrated that the exterior Galerkin procedure is identical to the least squares method. Thus the method of least squares is also applicable.

The stress functions are all compatible and satisfy equilibrium throughout the interior of the considered body.

Three types of stress functions, polynomial stress functions, closed form solutions from the classical theory of elasticity and singular stress functions from fracture mechanics were used and included in the computer program. The singular stress functions, closed form solutions, and the polynomial stress functions are combined where appropriate to improve the solution.

Based on the principle of superposition it follows that the Mode I stress intensity factor is given by the

sum of the Mode I stress intensity factors of each individual stress function used to describe the stress-field. From the definition of the stress intensity factors (see Chapter 3, equation 21) it follows that only stress functions which are singular at the leading edge of the crack have non-zero stress intensity factors.

The Galerkin procedure shows two distinct advantages compared with the available three dimensional methods. It is relatively a simple process with a single step solution, and is also applicable for studies of the interaction of cracks. The only limitation to this method is that one must use appropriate stress functions defining the stress field as adequately as possible.

The scope of this dissertation is to demonstrate the applicability of this general method to known cases and to evaluate the stress intensity factors for several structural details if possible. The features of the computer program are outlined and suggestions for further studies are given.

2. A GALERKIN METHOD FOR ELASTIC STRESS ANALYSIS

2.1 Mathematical Formulation of the Galerkin Method

As a numerical approximation technique, the Galerkin method belongs to the group of methods, using weighted residuals.

These methods have been reviewed by Desai[15] in a recent book by Finlayson[17]. The fundamental equation defining the method of weighted residuals is given by

$$\int_r w_r(x)\ r_r(x)\ dx + \int_b w_b(x) r_b(x) da = 0 \qquad (3)$$

r_r and r_b represent the residuals in the region r and on the boundary b. w_r and w_b are the corresponding weighting functions. If the method is used as a boundary method, the residual in the region is identically zero, since each of the selected functions satisfies the governing equations. In case the boundary residual is identically zero, the method is an interior method, where the boundary conditions are exactly satisfied by the selected functions. If the selected functions do not, in general, satisfy either the governing equations or the boundary conditions, the method is called a mixed method.

The stress analysis described in this dissertation uses the Galerkin method as an exterior or a boundary method.

The governing equations inside the region are represented by the equilibrium and compatibility equations, which are both satisfied by the selected stress functions. At any point inside the region the state of stress is described by a set of n linearly independent stress functions

$$\sigma = \sum_{i=1}^{n} \sigma_i \alpha_i \qquad (4)$$

σ_i are selected stress functions with parameters α_i, which are continuous throughout the entire region, satisfying equilibrium and compatibility.

On the boundary the state of stress is defined by the given boundary stresses t.

The residual on the boundary is defined by

$$r_b = \left(\sum_{i=1}^{n} s_i \alpha_i \right) - t \qquad (5)$$

where s_i is the individual stress function, which is transformed into the directions of the boundary stresses. stresses.

The residual r_r inside the region is identically zero for the boundary method.

Inserting the selected stress functions as weighting functions, the fundamental equation for the exterior Galerkin method is given by

$$\int_b r_b \, w_b \, da = 0 \tag{6a}$$

with $$r_b = \left(\sum_{i=1}^{n} s_i \, \alpha_i \right) - t = s - t$$

$$s = \sum_{i=1}^{n} s_i \, \alpha_i$$

$$w_b = s$$

$$\int_b (s-t) \, s \, da = 0 \tag{6b}$$

s represents the sum of the stress functions transformed into the directions of the boundary stresses. The integration has to include the entire boundary surface s and the crack surfaces.

For comparison the least square method is introduced at this point. This approach minimizes the residual in some sense and is characterized by the following expression

$$\int_b (s-t)^2 da \rightarrow \text{minimum} \qquad (7)$$

where the square of the residual is minimized.

Equation 6a illustrates the mathematical principle of the Galerkin method. Collatz[16] defines it as a procedure in which the weighting functions and the residuals are orthogonalized. The n parameters of the approximating functions are determined as the solution to a set of n linear simultaneous equations.

The least square method given by Eq. 7 reveals another important feature of the exterior Galerkin method. If the boundary conditions are not described in the form of derivatives, both methods have identical systems of n linear simultaneous equations, defining the parameters. This is demonstrated in Appendix A1 with three approximating stress functions.

Since both methods have identical systems of parametric equations, they represent identical solutions, which was confirmed in Ref. 17. Thus the orthogonalization procedure of the exterior Galerkin method minimizes the square of the residuals, which means that the boundary stress conditions are satisfied in the mean and the error is minimized in some sense.

Both methods can be used to determine the stress function parameters. Once the coding of the computer pro-

gram is completed the least square method and the exterior Galerkin method are identical. The Galerkin method was used in this study.

When the Galerkin method is used as an interior method, or if the boundary conditions are described by derivatives, the least square method will differ from the Galerkin approach.

2.2 Matrix Formulation of the Exterior Galerkin Method

The matrix formulation of the exterior Galerkin method is given by

$$\int_b \{s-t\}^T \{s\} \, da = 0 \tag{8}$$

where the integration covers the total surface of the elastic solid with arbitrary geometrical shape including all crack surfaces. $\{s-t\}^T$ is the transposed boundary residual vector,

$\{s\}$ = sum of the transformed stress vectors of the entire set of stress functions satisfying compatibility and equilibrium throughout the interior of the solid

$\{t\}$ = boundary stress vector

The sum of the transformed stress vectors $\{s\}$ is defined as

$$\{s\} = \sum_{i=1}^{n_f} [R_s] \{\sigma\}_i \alpha_i \tag{9}$$

where

$\{\sigma\}_i$ = individual stress vector of the stress function i

$[R_s]$ = stress transformation matrix which transforms global stress vectors into the three directions of the considered boundary stress vector $\{t\}$

n_f = total number of stress functions

$[R_s]$ and $\{t\}$ are in general functions depending on the global coordinates, x, y, z.

If the boundary surface including the crack surfaces of the elastic solid is approximated by n_s planar surface elements, Eq. (8) becomes:

$$\sum_{j=1}^{n_s} \int_{b_j} \left(([R_s]_j \sum_{i=1}^{n_f} \{\sigma\}_i \alpha_i - \{t\}_j)^T [R_s]_j \sum_{k=1}^{n_f} \{\sigma\}_k \alpha_k \right) da_j = 0 \tag{10}$$

$[R_s]_j$ is constant on each individual surface element. Evaluation of the basic orthogonality equations leads to a matrix [C] and a vector $\{E\}$. The matrix [C] is the coefficient matrix and the vector $\{E\}$ is the weighted boundary stress vector. The $n_f \times n_f$ elements of matrix [C] and the n_f components of the vector $\{E\}$ are explicitedly defined by multiplications

$$C_{ik} = C(i,k) = \sum_{j=1}^{n_s} \int_{b_j} \{\sigma\}_i^T [R_s]_j^T [R_s]_j \{\sigma\}_k da_j$$

if $$[Q] = [R_s]_j^T [R_s]_j$$

then $$C_{ik} = \sum_{j=1}^{n_s} \int_{b_j} \{\sigma\}_i^T [Q]_j \{\sigma\}_k da_j \tag{11}$$

and $$E_k = \sum_{j=1}^{ns} \int_{b_j} \{t\}_j^T [R_s] \{\sigma\}_k da_j \tag{12}$$

Thus the orthogonalization procedure described by Eq. (10) can be set into the matrix equation

$$[C] \{\alpha\} - \{E\} = 0 \tag{13}$$

Equation (13) represents a set of linear simultaneous equations. Their solution yields the stress function parameters.

3. STRESS FUNCTIONS

3.1 Introduction

Since the efficiency of the exterior Galerkin method is affected by the choice of stress functions, they must be selected carefully. Consideration must be given to the particular nature of the stress field problem which is being solved.

In this chapter two groups of functions are examined. They are the polynomial stress functions and special stress functions. The special stress functions are well known explicit solutions from linear fracture mechanics which describe the stress singularities around elliptical cracks that are fully embedded in an infinite elastic solid. This type of special stress functions is called a singular stress function. Other special functions, which define non-singular local stress fields in the form of closed form solutions from the theory of elasticity are called classical stress functions. Two examples of such classical stress functions are the solution which describes the nonsingular local stress fields around an ellipsoidal void embedded in an infinite elastic solid and the three dimensional stress distribution in the half space, due to a uniform pressure and shear, acting over a rectangular area on the boundary plane.

The two groups of stress functions can be either combined or used alone to provide a solution when the exterior

Galerkin procedure is used. Whether or not these groups are combined depends upon the problem.

If there are no geometrical singularities, the polynomial stress functions alone may yield a good description of the stress field. In cases where stress intensity factors must be determined, both the polynominal stress functions and the special stress functions have to be taken into account, since the local effects are of considerable importance and dominate the solution.

3.2 Special Stress Functions

3.2.1 Singular Stress Functions

The three dimensional stress distribution was computed around an elliptical crack embedded in an infinite elastic solid using the equations developed by Kassir-Sih.[20] These computations were used to explain the distinct features of the singular stress functions that are used in linear fracture mechanics. These functions have an inverse square root singularity at the border of the crack. Table 1 shows the change of the singular stress fields for two different loading cases. Column 1 in Table 1 represents the radial distance r perpendicular to the leading edge of the elliptical crack. Columns 2 through 4 in Table 1a and columns 2 through 5 in Table 1b contain the nonzero components of the global stress vector defined in Fig. 1a for a uniform pressure applied to the crack surface. Column 6

shows the ratio of the square root of the distances r_2 and r_1 (see Fig. 1b). Column 7 gives the inverse ratio of stresses normal to the crack plane $\sigma_{zz_1}/\sigma_{zz_2}$. The second loading case considered a uniform tension applied at an infinite distance from the crack surface and perpendicular to it. The ratio of the stresses normal to the crack plane for this loading case are listed in Column 8. The stress distribution due to this loading case corresponds to the mathematical model used to describe an elliptical crack embedded in an infinite elastic solid when subjected to uniaxial tension. The last two columns show that the inverse square root proportionality condition is better satisfied for the second loading case. It is apparent that points must be located near to the crack border, in order to satisfy the similarity of the stresses to the inverse square root of the distance the crack border.

Table 2 illustrates another feature of this particular singular stress function - the existence of plane strain along the border of the crack. Irwin[19] realized the importance of this condition and was able to describe the three dimensional problem adequately as a two dimensional problem. This permitted him to determine the stress intensity factor for the crack opening mode.

The radial distance, r, perpendicular to the leading edge of the elliptical crack is given in Column 1.

Columns 2 and 3 show the percentage deviation of plane strain in the x direction for the first loading case, where uniform pressure was applied to the crack surfaces. The percentage deviations are defined at the bottom of Table 2.

The deviations for the second loading case is tabulated in the last two columns of Table 2. The results demonstrate that the plane strain condition is almost three times better for the case of uniform pressure acting on the crack surfaces.

The plane strain condition holds for all points on the crack plane that are close to the leading edge of an elliptical crack. If the reference point p_o (see Fig. 1) on the leading edge of the crack does not fall on the minor axis the global stress vector must be transformed as illustrated in Fig. 1c. This transformation consists of a rotation around the z-axis. This results in stresses that are parallel and perpendicular to the tangent l_{zt} through P_o. The stress distribution close to the leading edge of an elliptical crack was derived from the general solution in Appendix 4. The general solution was developed by Kassir and Sih.[20] K_I in equation A16 through A20 represents the stress intensity factor for Mode I at point P_o.(See Equation 22). The angle ω is zero for points on the crack plane. This yields σ_{tt} equal to $-\nu \quad (\sigma_{zz} + \sigma_{nn})$

Hence, the condition of plane strain in the direction of the tangent ℓ_{zt} is satisfied.

3.2.1.1 Three Dimensional Stress Distribution Around an Elliptical Crack Embedded in an Infinite Elastic Solid

3.2.1.1.1 Crack Surfaces Subjected to Uniform Pressure

The most popular solution to this problem was given by Green and Sneddon[18]. Later Kassir and Sih[20] confirmed the analytical expression and extended the solution to the loading condition of uniformly distributed shear at an arbitrary angle. For convenience the notation used by Kassir and Sih will be adopted with minor modifications in this study[20].

The basic integral for the solution is given by

$$h = \frac{c_1}{2} \int_{\xi}^{\infty} \left[\frac{x^2}{a^2 + s} + \frac{y^2}{b^2 + s} + \frac{z^2}{s} - 1 \right] \frac{ds}{[Q(s)]^{1/2}} \qquad (14)$$

the stresses are found in terms of derivatives h:

$$\sigma_{xx} = h_{,xx} + 2\nu h_{,yy} + z\, h_{,zxx} \qquad (15)$$

$$\sigma_{yy} = h_{,yy} + 2\nu h_{,xx} + z h_{,zyy} \tag{16}$$

$$\sigma_{zz} = -h_{,zz} + z h_{,zzz} \tag{17}$$

$$\sigma_{zy} = z h_{,yzz} \tag{18}$$

$$\sigma_{zx} = z h_{,xzz} \tag{19}$$

$$\sigma_{xy} = (1-2\nu) h_{,xy} + z h_{,xyz} \tag{20}$$

The constant c_1 in Eq. (14) is defined by:

$$c_1 = -\frac{ab^2 p}{2 E(k)}$$

a = major half axis

b = minor half axis

p = constant pressure acting on the crack surfaces

$k = [1-b^2/a^2]^{1/2}$

$E(K) = \int_0^{\pi/2} [1-k^2 \sin u]^{1/2} du$ = complete elliptical integral of second kind

The expressions for the derivatives of h are given in Appendix 2 of (20) on pp. 609-610.

Once an analytical expression is established for the stress σ_{zz} normal to the plane of the crack (Eq. 17),

the stress intensity factor can be computed. K_I is defined by

$$K_I = \lim_{r \to 0} [(2\pi r)^{1/2} \sigma_{zz}] \quad (21)$$

at $z = 0$

By describing r with ellipsoidal coordinates and evaluating the limit of σ_{zz}, Shah and Kobayashi[21] found a solution identical to Irwin[19] for the stress intensity factor for the crack opening mode:

$$K_I = \frac{p}{E(k)}\left[\frac{\pi b}{a}\right]^{1/2}[a^2 \sin^2\theta + b^2\cos^2\theta]^{1/4} \quad (22)$$

For the two points located on the minor axis this expression yields at $\theta = \pi/2$,

$$K_I = \frac{p}{E(k)}[\pi b]^{1/2} \quad (23)$$

3.2.1.1.2 Crack Surfaces Subjected to Uniform Shear Parallel to the Major Axis

Kassir and Sih[20] developed a solution for uniform shear at an arbitrary angle ω to the major axis of the elliptical crack. It is more convenient with the exterior Galekin method, to treat this loading as two inde-

pendent loading conditions; shear parallel to the major axis and shear parallel to the minor axis. The analytical expressions for the stress can be expressed in the following form. The solutions were taken from(20) p. 603 and the following form substituted, $F = \partial f/\partial x + \partial g/\partial y$. This yielded:

$$\frac{\sigma_{xx}}{2\mu} = - 2 f_{,xz} - 2 \nu g_{,yz} + z [f_{,xxx} + g_{,xxy}] \tag{24}$$

$$\frac{\sigma_{yy}}{2\mu} = - 2 g_{,yz} - 2 \nu f_{,xz} + z [f_{,xyy} + g_{,yyy}] \tag{25}$$

$$\frac{\sigma_{zz}}{2} = z [f_{,xzz} + g_{,yzz}] \tag{26}$$

$$\frac{\sigma_{yz}}{2\mu} = - (1-\nu) g_{,zz} + \nu f_{,xy} + \nu g_{,yy} + z [f_{,xyz} + g_{,yyz}] \tag{27}$$

$$\frac{\sigma_{zx}}{2\mu} = - (1-\nu) f_{,zz} + \nu f_{,xx} + \nu g_{,xy} + z [f_{,xxz} + g_{,xyz}] \tag{28}$$

$$\frac{\sigma_{xy}}{2\mu} = - (1-\nu) f_{,yz} - (1-\nu) g_{,xz} + z [f_{,xxy} + g_{,xyy}] \tag{29}$$

The harmonic stress functions are defined by the basic elliptical integral

$$I = \frac{1}{2} \int_{\xi}^{\infty} \left[\frac{x^2}{a^2+s} + \frac{y^2}{b^2+s} + \frac{z^2}{s} - 1\right] \frac{ds}{[Q(s)]^{1/2}} \tag{30}$$

where $f(x,y,z) = c_2 I$

$g(x,y,z) = c_3 I$

For uniform shear parallel to the major axis, $g(x,y,z)$ and c_3 are identically zero. The nonzero constants c_2 are given by:

$$c_2 = \frac{ab^2k^2 q}{(k^2-\nu)E(k)+\nu\bar{k}^2K(k)} \tag{31}$$

q = uniform shear parallel to major axis

$k = [1-b^2/a^2]^{1/2}$

$\bar{k} = b/a$

$E(k)$ = complete elliptical integral of second kind

$K(k)$ = complete elliptical integral of first kind

The three dimensional stress distribution around an elliptical crack with the crack surfaces subjected to uniform shear q parallel to the major axis is given by:

$$f(x,y,z) = c_2 I \tag{32}$$

$$\frac{\sigma_{xx}}{c_2} = -2f_{,xz}+z\, f_{,xxx} \tag{33}$$

$$\frac{\sigma_{yy}}{c_2} = -2\nu f_{,xz}+2\, f_{,xyy} \tag{34}$$

$$\frac{\sigma_{zz}}{c_2} = z\ f_{,xzz} \tag{35}$$

$$\frac{\sigma_{yz}}{c_2} = \nu f_{,xy} + z\ f_{,xyz} \tag{36}$$

$$\frac{\sigma_{zx}}{c_2} = -\ (1-\nu) f_{,zz} + \nu f_{,xx} + z\ f_{,xxz} \tag{37}$$

$$\frac{\sigma_{xy}}{c_2} = -\ (1-\nu) f_{,yz} + z\ f_{,xxy} \tag{38}$$

and the mode two and three stress intensity factors become:

$$K_{II} = -\ \frac{c_2}{a}\ \left[\frac{\pi}{ab}\right]^{1/2} \cos\theta\ \left[a^2\sin^2\theta + b^2\cos^2\theta\right]^{1/4} \tag{39}$$

$$K_{III} = (1-\nu)\ \frac{c_2}{b}\left[\frac{\pi}{ab}\right]^{1/2} \sin\theta \left[a^2\sin^2\theta + b^2\cos\theta\right]^{1/4} \tag{40}$$

3.2.1.1.3 Crack Surfaces Subjected to Uniform Shear Parallel to the Minor Axis

When uniform shear is applied parallel to the minor axis, $f(x,y,z)$ and c_2 are identically zero. The constant c_3 becomes:

$$c_3 = \frac{ab^2\ k^2\ q}{(k^2+\nu\bar{k}^2)E(k) - \nu\bar{k}^2 K(k)} \tag{41}$$

$$g(x,y,z) = c_3\ I \tag{42}$$

and the stresses are given by the following expressions:

$$\frac{\sigma_{xx}}{c_3} = -2\nu\, g_{,yz} + z\, g_{,xxy} \tag{43}$$

$$\frac{\sigma_{yy}}{c_3} = -2\, g_{,yz} + z\, g_{,yyy} \tag{44}$$

$$\frac{\sigma_{zz}}{c_3} = z\, g_{,yzz} \tag{45}$$

$$\frac{\sigma_{yz}}{c_3} = -(1-\nu) g_{,zz} + \nu g_{,yy} + z\, g_{,yyz} \tag{46}$$

$$\frac{\sigma_{zx}}{c_3} = \nu g_{,xy} + z\, g_{,xyz} \tag{47}$$

$$\frac{\sigma_{xy}}{c_3} = -(1-\nu) g_{,xz} + z\, g_{,xyy} \tag{48}$$

The mode two and three stress intensity factors become:

$$K_{II} = -\frac{c_3}{b} \left[\frac{\pi}{ab}\right]^{1/2} \sin\theta \left[a^2 \sin^2\theta + b^2 \cos^2\theta\right]^{1/4} \tag{49}$$

$$K_{III} = -\frac{c_3}{a} (1-\nu) \left[\frac{\pi}{ab}\right]^{1/2} \cos\theta \left[a^2 \sin^2\theta + b^2 \cos^2\theta\right]^{1/4} \tag{50}$$

3.2.1.1.4 Crack Surfaces Subjected to a Polynominal Pressure Distribution in X and Y

The solution by Shah and Kobayashi[21] will be used for this loading case. If the crack is small and fully embedded compared to the boundary surface of the elastic solid, the coefficients of the pressure polynomial and the parameters of the singular functions, determined by the exterior Galerkin method ,are identical. On the crack surface the singular stress functions reduce to the pressure polynomial.

If the pressure polynomial is described in terms of the local coordinates of the crack coordinate systems, $\bar{X}$, and $\bar{Y}$ with $\bar{Z} = 0$, the polynomial is described by:

$$p(\bar{x},\bar{y}) = \alpha_1+\alpha_2\bar{x}+\alpha_3\bar{y}+\alpha_4\bar{x}^2+\alpha_5\bar{xy}+\alpha_6\bar{y}^2+\alpha_7\bar{x}^3+\alpha_8\bar{x}^2\bar{y}+\alpha_9\bar{xy}^2+\alpha_{10}\bar{y}^3 \tag{51}$$

$\alpha_1 \ldots \alpha_{10}$ = parameters of the singular stress functions determined by the exterior Galerkin method

For convenience the notation used in Ref. [3.4] was slightly modified as follows:

$$\phi_{00} = f_1, \phi_{10} = f_2, \ldots \phi_{03} = f_{10}$$

$$c_{00} = \gamma_1, c_{10} = \gamma_2, \ldots c_{03} = \gamma_{10}$$

and the matrix

$$[S_K]\{\gamma\} = \frac{1}{2G}\{\alpha\} \tag{52}$$

Once the singular stress function parameters $\{\alpha\}$ are determined with the exterior Galerkin Method, the coefficients to the stress functions can be obtained by the multiplication of the inverted matrix $[S_K]$ and $\{\alpha\}$

$$\{\gamma\} = \frac{1}{2G}[S_K]^{-1}\{\alpha\} \tag{53}$$

The mode I stress intensity factor is described in terms of $\{\gamma\}$'s and becomes

$$K_I = \frac{8G}{ab}\left(\frac{\pi}{ab}\right)^{1/2}(a^2\sin^2\theta+b^2\cos^2\theta)^{1/4}\ \gamma_1+\frac{\gamma_2\cos\theta}{a}+$$

$$\frac{\gamma_3\sin\theta}{b}-\frac{4\gamma_4\cos^2\theta}{a^2}+\gamma_5\frac{\cos\theta\sin\theta}{ab}-4\gamma_6\frac{\sin^2\theta}{b^2}-4\gamma_7\frac{\cos^3\theta}{a^3}$$

$$-4\gamma_8\frac{\cos^2\theta\sin\theta}{a^2b}-4\gamma_9\frac{\cos\theta\sin^2\theta}{ab^2}-4\gamma_{10}\frac{\sin^3\theta}{b^3} \tag{54}$$

3.2.2 Classical Solutions from Theory of Elasticity

For completeness some solutions to stress field problems are listed, which must be used if the stress in-

tensity factors for surface flaw problems are computed with the exterior Galerkin method.

Whenever a free surface is intersected by an elliptical crack, two points on the free surface are common with two points on the border of the elliptical crack. This means that the stresses at these locations are singular. In the neighborhood of these points, the stresses are very large, but decrease very rapidly with increasing distance from the singular points as was demonstrated in Table 1. Since polynomial stress functions are inefficient when approximating such highly localized stress fields, special stress functions must be added. If the crack intersects just one free surface plane, and the back surface plane is parallel to the front surface plane of the crack, Love's stress functions (23) together with Shah and Kobayashi's solution(22) can be used to take the free surface effect into account. Figure 2 shows the assignment of special stress functions to a rectilinear mesh. The mesh must be carefully designed so that the steepness of the stress field is accounted for. For illustration, consideration is only given to the front surface plane. This plane is also subjected to shear stress under arbitrary nonsymmetric loading conditions.

When two surface planes intersect at an angle less than π radians and the major axis of the elliptical

crack is on the line of intersection. Mindlins stress function (see Ref. 24) will be used instead of Love's. The reference free surface for these stress functions must be assumed far enough away from the actual surface in order to restore the local nature of the discontinuity.

For stress field problems which have geometrical discontinuties, such as cavities or pores in welds, the solution by Sadowsky and Sternberg[25] is used. This solution considers an ellipsoidal void embedded in an infinite elastic solid subjected to arbitrary plane stress.

3.3 Polynominal Stress Functions

3.3.1 Introduction

Polynomial stress functions have two distinct features which permit efficient computer application. According to the Weierstrass principle [28] any continuous function can be approximated uniformly with arbitrary accuracy by a series of polynomials. In addition, polynomial functions are simple to differentiate and integrate and can be automatically generated.

Whenever functions are used to describe stress fields, they must satisfy equilibrium and compatibility. It is difficult to construct three-dimensional polynomial stress functions for anisotropic materials, which satisfy

both conditions simultaneously. In this section a procedure is described which permits the polynomial stress functions to be developed by satisfying equilibrium alone. The functions can also be made to satisfy the compatibility conditions with a matrix transformation if desired.

This compatibility transformation was proposed by Desai[26], who also developed a computer program for the automatic generation of three dimensional polynomial stress functions.

While polynomial stress functions can be constructed using the Papkovitch-Neuber approach[27] for isotropic material, the method proposed by Desai[26] is more general and is also applicable to anis otropic homogeneous materials. A comparison of the number of polynomial stress functions resulting from the Papkovitch-Neuber and Desai approach is given in Table 4.

3.3.2 Polynomial Stress Functions that Satisfy Equilibrium

A polynomial stress function $\{\sigma\}_i$ will be defined as

$$\{\sigma\}^T_i = \{\sigma_{xx}, \sigma_{yy}, \sigma_{zz}, \sigma_{yz}, \sigma_{zx}, \sigma_{xy}\} \quad \alpha_i \qquad (55)$$

in which each of the six stress components is represented by the following polynomial

$$\sigma_j = a_j \, x^k \, y^m \, z^n \alpha_i \tag{56}$$

where

α_i = stress function parameter

a_j = coefficient

$x^k . y^m . z^n$ = polynomial coordinate function (this type of polynomial was selected for convenience)

The complete set of polynomial stress functions correspondent to a specific power k+m+n, can be constructed using the following procedure.

First, all of the possible power combinations k, m, n are systematically inserted into each stress component as is apparent in Appendix A2. The complete set of functions up to the second power are listed. By satisfying the equilibrium condition given by Eq. 57

$$\begin{aligned} \sigma_{xx,x} + \sigma_{yx,y} + \sigma_{zx,z} &= 0 \\ \sigma_{xy,x} + \sigma_{yy,y} + \sigma_{zy,z} &= 0 \\ \sigma_{xz,x} + \sigma_{yz,y} + \sigma_{zz,z} &= 0 \end{aligned} \tag{57}$$

the coefficients a_j are determined and all linearly dependent functions can be deleted.

Table 3 provides a comparison between the total number of linear independent polynomial functions resulting from the displacement field and the stress field approach. The polynomial functions from the stress field formulation must be compared with one order higher functions of the displacement field, since the stresses are related to the strains by the compliance tensor. The strains are defined by the first derivatives of the displacements in linear elastic problems. If the displacement field and the stress field describe the same problem, the corresponding number of net functions must be identical. This is the case as is illustrated in Table 3.

3.3.3 Compatibility Transformation of Polynomial Stress Functions that Satisfy Equilibrium

If all polynomial stress functions which satisfy equilibrium are substituted into the compatibility equations listed in Appendix A3, an equivalent number of homogeneous equations can be generated. These equations relate some of the polynomial stress function parameters α_i to each other.

The polynomial defined by Eq. 54 yields stress functions that produce some linearly dependent compatibility equations. These linearly dependent equations result from the polynomial stress function that have powers greater than two. For example Table 3 shows the number of

linearly dependent compatibility equations in Column 5. All linearly dependent equations must be eliminated.

The equations define a linear relationship between values of α. These equations can be used to construct the transformation matrix $\bar{R}$. It permits function parameters α_i to be reduced into a smaller number of new parameters $\bar{\alpha}_i$. The reduced set of parameters, $\bar{\alpha}_i$, are defined by a linear combination of the parameters α_i. The number of reduced parameters is the difference between the number of α_i and the number of linearly independent compatibility equations. The relationship of the reduced parameters $\bar{\alpha}_i$ to the original parameters, α_i, is defined in matrix form by:

$$\{\bar{\alpha}_o\} = [\bar{R}]\{\alpha\} \tag{58}$$

In order to express the α's in terms of $\bar{\alpha}$, the matrix $[\bar{R}]$ must be inverted. This means $[\bar{R}]$ must be square and its determinant non-zero. To construct $[\bar{R}]$, the first step is to add to the reduced parameters $\bar{\alpha}$ as many zero parameters as there are linear independent compatibility equations. The next step is to insert the elements in $[\bar{R}]$ which are located in those rows corresponding to the zero parameters in $\{\bar{\alpha}\}$. Every row which has $\alpha = 0$ corresponds to a compatibility equation. As illustrated in Fig. 3 this results in a set of linear homo-

geneous equations. The remaining elements can be arbitrarily selected but must provide a non-singular matrix $[\bar{R}]$. One possibility is to define all remaining elements as zero except those elements which fall on the two diagonals indicated in Fig. 3. Matrix $[\bar{R}]$ is now square and can be inverted. Hence, $\{\alpha\}$ can be defined in terms of $\{\bar{\alpha}\}$ as:

$$\underset{nx1}{\{\alpha\}} = \underset{nxn}{[\bar{R}]^{-1}} \underset{nx1}{\{\bar{\alpha}\}} \qquad (59)$$

Once matrix $[\bar{R}]$ is established and inverted, the rows corresponding to the reduced zero parameters can be deleted from the inverted matrix. This results in the matrix [R] for compatibility transformation.

Matrix [R] is no longer square, but is more convenient to use since the reduced zero parameters have been omitted and the relationship between $\{\alpha\}$ and $\{\bar{\alpha}\}$ is given by:

$$\underset{nx1}{\{\alpha\}} = \underset{nxn_R}{[R]} \underset{n_R x1}{\{\bar{\alpha}\}} \qquad (60)$$

For efficiency it is necessary to assemble the polynomial stress functions into complete sets corresponding to a specific power and to perform the compatibility transformation in submatrices. The generation of these submatrices is illustrated in Fig. 4 for second order polynomial

stress functions. The number of α's is 27 and the number of linearly independent compatibility equations is 6 which yields 21 reduced parameters $\bar{\alpha}$.

Polynomials with powers less than two are always compatible. Thus they yield unit diagonal transformation submatrices. Fig. 5 shows the assembled compatibility transformation matrix [R] for twenty special stress functions and all polynomial stress functions up to the third power. The compatibility transformation of the polynomial stress function influences the Galerkin procedure described in Chapter 2.

Starting with the basic matrix equation that defines the stress function parameters α, (see Eq. 13) the compatibility transformation can be implemented as follows:

$$[C]\{\alpha\}-\{E\} = 0 \tag{61}$$

$$\{\alpha\} = [R]\{\bar{\alpha}\} \tag{62}$$

$$[R]^T[C][R]\{\bar{\alpha}\}-[R]^T\{E\} = 0 \tag{63}$$

$$[R]^T[C][R] = [\bar{C}] \tag{64}$$

$$[R]^T\{E\} = \{\bar{E}\} \tag{65}$$

$$[\bar{C}]\{\bar{\alpha}\}-\{\bar{E}\} = 0 \qquad (66)$$

The coefficient matrix [C] and the weighted boundary stress vector {E} can be reduced to $[\bar{C}]$ and $\{\bar{E}\}$. The system is then solved for the reduced parameters $\{\bar{\alpha}\}$.

Once the reduced parameters $\{\bar{\alpha}\}$ are determined, the parameters $\{\alpha\}$ can be obtained by the transformation provided by Eq. (58).

The procedure can be summarized as follows: first the original coefficient matrix [C] and the weighted boundary stress vector {E} are generated. These are transformed into $[\bar{C}]$ and $\{\bar{E}\}$ and the reduced system is solved for $\{\bar{\alpha}\}$. Finally values of $\{\alpha\}$ are obtained by the transformation equation (58).

In the computer program the generation and reduction process is performed on submatrices. Figure 6 shows the partitioning of the coefficient matrix [C] with submatrices. These submatrices represent the special functions and each set of powers of the polynomial stress functions. The solution of the linear simultaneous equations is based on Choleshi decomposition. The solution and reduction process was developed by Desai [26].

For simplicity one additional requirement for the compatibility transformation matrix has been omitted and

shall be mentioned now. If matrix [C] in Eq. (60) is positive definite, which is in the Galerkin method always the case, the reduced matrix $[\bar{C}]$ must also be positive definite or the matrix $[R]^T \cdot [R]$ must be positive definite.

The compatibility transformation matrix satisfies this requirement. Desai[26] has suggested an additional transformation so that the matrix product $[R]^T[R]$ is orthonormalised. This is believed to yield better transformation matrices from the numerical point of view.

CHAPTER 4

APPLICATION OF METHOD TO SEVERAL MODELS

4.1 Studies of a Hexahedron with a Symmetrically Embedded Elliptical Crack

This simple model was selected to demonstrate the applicability of the Galerkin method. Among the variables investigated were the effect of crack size, special weighting of the crack surfaces, and the interaction of the boundary surface of the solid with the crack surface.

Figure 7 shows the model dimensions and the loading. A uniform tension was applied to the top and bottom surfaces of the hexahedron.

Figure 8 defines the points at which resultant surface stresses were computed to demonstrate the accuracy of the result. Points 1-5 were selected on the crack surface. The schematic stress distribution on the crack surface is illustrated at sections A-A, B-B, and C-C, for polynomial stress functions up to power 2 and the singular stress function defined in Chapter 3, 3.2.1.1.1. Points 6-7 are located on the front, points 10-11 on the profile and points 8 and 9 on the top surfaces of the hexahedron.

The numerical results are summarized in Tables 5-8 for elliptical crack sizes that have elliptical axis

which vary from 1/20 (CX = 0.1, AX = 2.0, CY = 0.05, AY = 1.0) of the cross section up to 1/2 of the cross section. All eleven points shown in Fig. 8 are tabulated. Each column in Tables 5-8 shows the surface stress S_{33} in the normal direction. The shear stresses S_{13} and S_{23} are not listed in the tables. However, the results were in good agreement. They were equal in magnitude between 0 and $\pm$ 1.0×10^{-14}, which confirmed that symmetry was indeed satisfied. All results were obtained using polynomial stress functions up to power 2 and the singular stress function defined in Chapter 3, 3.3.1.1.1.

To assist with the evaluation of the significance of the crack surfaces, various weights (WELCR) were assigned to the surface element which represented the crack. No matter how small the crack is compared to the dimension of the model, any resultant stress distribution on the crack surfaces will significantly influence the stress intensity factors.

In generating the coefficient matrix and the weighted boundary stress vector all integrations were performed over the total surface of the model, including the crack surfaces.

When the crack size is very small compared to the model dimension, the contribution of the crack surfaces

will vanish. It was concluded that equal attention should be given to the crack surface and the total boundary surface of the model. A special weight factor (WELCR) was assigned to the crack surfaces.

The interaction of the boundary surface of the model with the crack surfaces is indicated by the singular stress function parameter α_1. This parameter becomes unity for infinite model dimensions. From the definition of the stress intensity factor (see Chapter 3, Eq. (21) it follows, that the stress intensity factor for finite model dimensions is obtained from the product of the stress intensity factor for the infinite solid and the singular stress function parameter α_1. Thus, α_1 provides a correction factor for finite model dimensions.

Table 5 shows the resultant residual stress distribution on the boundary surfaces at the 11 points specified in Fig. 8. The crack size was 1/20 of the cross section. Each column represent the stress components S_{33} normal to the crack surface. Four different weight factors, WELCR, ranging from 1.0 to 100,000.0 were assigned to the crack surface. All yielded α_1 equal to 1.000. This indicates that the crack size is small enough so that the boundary surfaces have no effect. A condition comparable to infinite model dimensions is reached.

Table 6 summarizes the result of a similar computation for a crack which was 1/8 of the cross section dimensions. The special weight factors that were applied to the crack surface were 1.0, 720.0, and 720,000.0. All α_1 factors were again unity, which indicated that the free boundary surfaces had no effect even though the crack size was 1/8 of the cross section dimension. The resultants residual stress distribution also indicated that the selected stress functions provided a satisfactory description of the stress field.

Table 7 summarizes the results obtained with a crack size equal to 1/4 the cross section dimensions. Four different weight factors were used: 1.0, 180.0, 1,800.0, and 2,000,000.0. In this example the finite model dimensions are seen to have an effect. The values of the α_1 parameters were not greatly affected by weight factor even with a variation from 1.0 up to 2,000,000.0.

The resultant residual stress distribution that remained on the boundaries and crack surface were negligible. Hence, the assumed stress functions described the stress field satisfactorily for a crack size equal to 1/4 the cross section dimensions.

A crack size equal to 1/2 the cross section dimensions was also examined. Four different weight fac-

tors were used: 1.0, 10.0, 100.0, and 1,000.0. The results are summarized in Table 8. The values of the singular stress function parameters α_1 are still very stable for all weight factors. A comparison of the results with the smaller crack size show that the resultant residual stress distribution on the boundaries and crack surfaces have increased. This is a result of the finite model dimensions with the larger crack size a substantial disturbance of the stress field results. This is caused by the singularity along the border of the elliptical crack. The stress distribution at point 6 is much larger than the value at point 7 since point 6 is located on the plane of the elliptical crack along the minor axis.

Figures 9 and 11 show schematically the results summarized in Table 8. It is readily apparent that the residual stress distributions were not greatly effected by the different weighting factors. A solution was also obtained for a weight factor of 40. This weight factor made the crack surfaces equal in magnitude to the total boundary surfaces of the body. The results of this solu- are summarized in Fig.10. It is readily apparent that comparable results were obtained for special weighting factors on the crack surfaces that were greater than unity.

The effect of higher order polynomial stress functions was also investigated. The results are summa-

rized in Table 9 and Fig. 12. Figure 12 shows the results obtained for the crack size and model dimensions given in Table 8. The polynomial stress functions were increased to the third power and combined with the singular stress function. The results are identical with those summarized in column 5 of Table 8. It is also apparent from a comparison of Figs. 11 and 12 that nearly comparable results were obtained when a weight of 100 was used with a second power polynomial. This agreed with the theory, since symmetric models must have zero antisymmetric terms when polynomial stress functions are used.

Table 9 summarizes the results obtained for an elliptical crack size equal to 1/2 the cross section of the model (see Table 8). A weight factor, WELCR of 40.0 was used so that comparisons could be made with other studies (22). The polynomial stress functions were used with the same singular stress function . Two different powers of polynomial stress functions were used (power 2 and power 4). In both cases the odd sets of polynomial stress functions were omitted and the compatibility transformation bypassed. The central processor time was about 90 sec. for power 2 and 300 sec. for power 4 on a CDC 6400 computer.

The results summarized in Table 9 show two important facts. First there is little effect on the re-

sultant stress distribution and the singular stress function parameter α_1 when the polynomial stress functions are not compatible. This means that the polynomial stress functions only satisfied the equilibrium conditions. The compatibility equations were not considered. The results given in column 2 of Table 9 for second power polynomial stress functions and a weighting factor of 40 are directly comparable to the results given in Fig. 10.

Second the resultant stress distribution on the boundary and crack surfaces is not an indication of the accuracy of the computer singular stress function parameter α_1. The results obtained with fourth power polynomial stress functions are listed in the second column of Table 9. Although the resultant stress distribution on the boundary and crack surface are slightly larger than obtained with the second power polynomial stress functions, the value of α_1 is improved. Considering the order of magnitude of the resultant stress distribution it can be concluded that both second and fourth power polynomial stress functions describe the stress field satisfactorily.

The resultant stress distribution on the boundary and crack surfaces may indicate the accuracy of the numerical solution. If the pressure polynomial that is applied to the crack surface has the same order as the maximum

power of the polynomial stress functions, then the resultant stress distribution will be improved. Some local disturbance may still remain if no additional special stress functions are also reached.

A reasonable estimate of the actual singular stress function parameter α_1 is:

$$\alpha_1 = 1.03 \pm 0.01$$

This value is in good agreement with the results obtained by Shah and Kobayashi on an elliptical crack embedded in a semi infinite solid. They found the correction factor to be: 1.02 ± 0.01.

In this study attention was also given to the effect of partial interaction of the singular stress functions with the polynomial stress functions.

The partial interaction effect was achieved during the generation of the coefficient matrix. All submatrices corresponding to either pure special stress-functions or the mixed special - polynomial stress functions were generated by limiting all integration procedures to the crack surfaces.

Partial interaction between singular and polynomial stress functions was examined with the large crack and model dimensions given in Table 8. Two examples were

evaluated. The first considered that compatible polynomial stress functions up to the power 2 and the singular stress functions described in Chapter 3, 3.2.1.1.1. In the second example compatible polynomial stress functions up to power 2 were used with the Shah-Kobayashi third degree pressure polynomial (see Chapter 3, 3.2.1.1.4).

The results of both investigations were consistent and comparable. The first case yielded α_1 equal to unity. In the second case all singular stress function parameters were zero except the first one, which corresponded to uniform pressure. This parameter was also unity.

Based on the principle of superposition it follows that the stress intensity factor is given by the sum of the stress intensity factors of each individual stress function that was used to describe the stress field. From the definition of the stress intensity factor (see Chapter 3, Equation31), it follows that only singular stress functions have non-zero stress intensity factors. Thus the stress intensity factors for finite model dimensions are given by the sum of the products of each individual stress intensity factor for infinite solid and the associated singular stress function parameter x_i that were obtained for the finite solid.

4.2 Hexahedron with Embedded Eccentric Elliptical Crack

The effect of eccentricity of the crack was examined with a three dimensional solid having a semi-elliptical crack as shown in Fig. 13.

The results listed in Table 10 were obtained for a semi-elliptical crack width axis equal to 1/2 the model cross section dimensions. A special weight factor on the crack surfaces of 100.0 was used. Compatible polynomial stress functions up to power 2 with the singular stress function of uniform pressure acting on the crack surface was considered.

Since no special stress functions (see Chapter 3, 3.2.2) have been included to account for the three-dimensional singularities at the intersection of the elliptical crack with the free surface, the result does not represent a solution to the surface crack.

The points at which the resultant stress distribution was computed are defined in Fig. 13. Points 1-5 were located on the crack surface point 6 and 7 on the top surface, points 8 and 9 on the profile, opposite to the crack, and points 14 and 15 on the front surface. Points 10-13 were laying on the profile intersecting the crack surface. Points 11 and 13 were positioned close to the

three dimensional singularities, to demonstrate this highly localized feature of surface cracks.

The normal stress at points 11 and 12 were reduced to 16.95 even though these points are only 1/50,000 of the minor half axis above the singular points.

The example demonstrates that the polynomial stress functions give a reasonable description of the stress field even when the crack is eccentrically embedded.

The result also shows that the polynomial stress function cannot yield a reasonable description of the stress field when a surface flaw exists. They cannot remove the high stress close to singular points.

4.3 Structural Details with Complex Geometry

The studies summarized in Arts. 4.1 and 4.2 show that the solution technique provides reliable results for prismatic members without geometric discontinuities and surface flaws. The method was also applied to several complex details to ascertain whether or not the approach could be used to estimate the stress field and stress intensity factors.

A T-shape with a coverplate attached to the

flange was selected for one detail as shown in Fig. 14. This represented a commonly used structural detail which has been extensively studied under both static and fatigue loading conditions.

Figure 14 shows the detail geometry and the location of points at which the 3-dimensional state of stress was computed. The cross-section dimensions and the loading conditions which were examined in this study are shown in Fig. 15. Two different stress fields were applied to the cross section. One simulated the bending stress gradient in a beam (Model 5-1) and the second corresponded to a uniformly stressed cross section.

A semi-elliptical crack was introduced at point one and treated as a fully embedded crack. All local stress singularities at the interaction with the free surface were ignored. A uniform pressure singular stress function was applied to the crack surfaces. Compatible polynomial stress functions up to the second power were assumed to approximate the stress field. Since the crack dimensions (major axis = 0.01117 in. and minor axis = 0.01 in.) were very small compared to the total geometry of the model, partial interaction between singular stress functions and polynomial stress functions was assumed.

The results of the analysis are summarized in Table 11. It is readily apparent from the results given in Table 11 that the stress field predicted by the method is not satisfactory. Even the stress at the boundary of the plate at locations 7 and 8 is not in agreement with the applied stress field. The stresses generated along the weld toe at points 1-6 are not reasonable. The approach does not appear to be applicable with lower power polynomials to complex geometries.

It is possible that these absurd stress distributions are results of the asymmetry of the model and insufficient powers of the polynomial stress functions. The polynomial stress functions are too smooth to account for the stress field irregularities.

A simpler detail was examined to determine whether or not this would improve the solution. A non-load carrying cruciform joint was used as shown in Fig. 16. All local singularities at corner points were ignored. The cruciform joint was examined for two crack conditions. Model 3-1 considered a semi-elliptical crack embedded at point 1 in Fig. 16. Model 3-8 considered the case of eight semi-elliptical cracks embedded near points 1, 3, 4 and 6 on each surface. Studies were also made on a specimen without any embeeded cracks (Model 3). In

Model 3-1 and Model 3-8 singular stress functions and uniform pressure was applied to each individual crack surface. These were used with second power compatible polynomial stress functions. The same crack dimensions were used for all studies. In addition, partial interaction between the singular stress functions and the polynomial stress functions was assumed. The cruciform arms for Model 3-1 were taken as 12 inches long. For Model 3-8 and Model 3 these arms were assumed to be 0.625 inches long as shown in Fig. 16.

The result obtained with Model 3-1 and Model 3-8 are summarized in Table 12. It is readily apparent that method of analysis did not provide satisfactory results.

The method was further examined by removing all embedded cracks as illustrated in Fig. 16 for Model 3.

Since Model 3 was now fully symmetric and contained no cracks all odd sets of the polynomial stress functions were eliminated. Table 13 summarizes the results obtained with second and fourth power polynomial stress functions. The compatibility transformation was not considered and only the equilibrium conditions were satisfied.

The results summarized in Table 13 indicate that neither solution provided a satisfactory stress distribution in the body. There appeared to be a slight increase

in the stress field provided by the fourth power polynomials.

A final study was made on a hexahedron with a cylindrical hole as illustrated in Fig. 17. The loading and points at which the stress distribution was evaluated are shown in Fig. 15. The geometry of this model permitted the use of a plane strain closed form solution from the theory of elasticity.[30] This described the stress field around a cylindrical hole in an infinite plate. This solution was used as a special function together with the polynomial stress functions.

Table 14 summarizes the results obtained with compatible polynomial stress functions up the second power. The result using polynomials alone is not satisfactory. A solution was also obtained using the special function for an infinite plate with a hole. The results of this solution are summarized in Table 15. The closed form solution of an infinite plate with a cylindrical hole was used with compatible polynomial stress functions up to power 2. A comparison of Tables 14 and 15 show that the stress field was improved. However, the results were not a satisfactory description of the stress distribution.

The results of the studies on solids with complex geometry suggest that the method is not satisfactory for

the polynomial stress functions used. The singularities that exist near points of geometric change cannot be described by the polynomial stress functions.

5. SUMMARY AND CONCLUSIONS

5.1 Summary and Features of the Computer Program

In this dissertation a Galerkin procedure was developed to approximate three dimensional stress fields and to compute stress intensity factors.

Chapter 3 lists the stress functions used in this dissertation to demonstrate the Galerkin procedure. Special attention is given to polynomial stress functions. References for special stress-functions, which must be considered in complex problems are also listed in Chapter 3.

The application of the Galerkin method to several models is described in detail in Chapter 4. The Galerkin procedure is described in Chapter 2.

A general computer program was developed using the Galerkin method with polynomial and singular stress functions for numerical computations of the stress field and stress intensity factors in structural details. One part of the program was developed by Desai.[26] This included the automatic generation of polynomial stress functions, the computation of compatibility transformation - matrices and the Choleski decomposition solution technique for the system of simultaneous linear equations.

The computer program includes polynomial stress functions up to the seventh power, three singular stress function routines, and one subroutine for a closed form solution from the classical theory of elasticity. The singular stress functions describe the local stress field around an elliptical crack subjected to uniform pressure and shear in both directions of the principle axis, according to Kassir-Sih.[20] The classical solution defines the plane strain stress distribution around a cylindrical hole in an infinite plate, subjected to uniform, uniaxial tension at infinity. The Shah-Kobayashi pressure polynomial acting on the surfaces of an elliptical crack is also included in the program with the limitation of partial interaction as described in Chapter 4, paragraph 4.1. The subroutines defining the singular stress functions that were developed by Kassir and Sih[20] cannot be used for penny-shaped cracks (major half axis a = minor half axis b) and cracks with b smaller than 0.0005 in.

The structure of the computer program permits updates of additional routines such as LOVE's stress functions without major modifications.

The following boundary stress problems were used to test the applicability of the Galerkin procedure:

1. Hexahedron with symmetrically embedded crack

subjected to uniform tension (Fig. 7).

2. Hexahedron with eccentrically embedded crack subjected to uniform tension (Fig. 13).
3. Simple weld detail, a crucifix specimen subjected to uniform tension (Fig. 16).
4. T-shaped specimen with flange cover-plate subjected to uniform bending as well as uniform tension (Fig. 14).
5. Hexahedron with cylindrical hole subjected to uniform tension (Fig. 17).

5.2 Conclusions and Suggestions for Future Research

The results of the boundary stress problems examined in this study permit the following conclusions to be made:

1. Polynominal stress functions are too smooth to describe locally disturbed stress fields.
2. When combined with special stress-functions describing the local nature of a disturbed stress field, polynomial stress functions provide a good tool to smooth out the resultant stress-distribution and to reduce the error on the boundary surface.
3. The Galerkin procedure using uniform pressure acting on the crack surface and polynomial

stress functions yields reasonable and efficient results for stress intensity computations in prismatic bodies for a symmetrical interior crack.

4. Ignoring the compatibility transformation of polynomial stress functions does not materially influence the results.
5. The condition of infinite body dimensions with respect to the crack size is satisfied for elliptical cracks embedded in prismatic bodies if the crack size is less than 1/8 of the cross-section dimension.
6. Special weighting of the crack surface yields no substantial changes in the resulting stress function parameters, but does slightly improve the resultant stress distribution on the boundary and crack surfaces.
7. Incomplete interaction between singular and polynomial stress functions is equivalent to infinite body dimensions.
8. The values of the resultant stress-distribution on the boundary and crack surfaces are not an indicator of the accuracy of the method.
9. The values of the resultant stress distribution on the boundary and the crack surfaces

yield some indication of the relative accuracy of the procedure with regard to the selected stress-functions.

10. The stress intensity factors for finite model dimensions are given by the sum of the products of the individual stress intensity factors for an infinite solid and the associated singular stress function parameters α_i.

11. A deviation from plane strain equal to 18 to 26 percent was found at distances as small as 2 percent of the minor axis from the leading edge of an elliptical crack. However, the stress state in this region remains approximately one of generalized plane strain, that is the gradient of the extensional strain parallel to the crack border is nearly zero.

12. The stress functions used by Smith,[13] Shah et al.[14] and Hartranft et al.[31] can also be used with the exterior Galerkin method. This avoids the necessity of an iterative solution and should also improve the accuracy of the numerical results.

13. Future studies are needed to determine if

the method can be improved and applied to complex geometrical solids.

Consideration should be given to improving the solution by considering the following factors:

- utilizing Love's stress functions to remove the stresses on free surfaces.
- using singular stress-functions to provide full interaction with the pressure polynomial suggested by Shah and Kobayashi.
- providing special functions which describe the local singularities that exist at corners.

Various types of stress functions should be examined so that the best description of the stress field can be provided for complex structural details.

Other factors such as the interaction of multiple cracks and the effect of geometrical discontinuities on the stress intensity factors need study when a satisfactory solution is finally available.

TABLE 1

The Inverse Square Root Singularity at the Tip of an Elliptical Crack

Stress distribution according to Chapter 3, 3.2.1.1.1, b = Minor Halfaxis, r = Distance from reference point, intersection of minor axis with crack tip.
Pressure on the crack surface p = -1.0, a = 1.0 b = 0.5

1a. Points Located on the Extension of the Minor Axis

$\sigma_{yz} = \sigma_{zx} = \sigma_{xy} = 0$ (Symmetry+Crack Plane)

(1) r	(2) σ_{xx}	(3) σ_{yy}	(4) σ_{zz}	(6) (1)	(7) (2)	(8) (3)
b/500,000	247.00	411.97	411.86	3.16	3.17	3.16
b/50,000	77.63	129.66	129.56	3.16	3.21	3.16
b/5,000	24.07	40.40	40.29	3.16	3.33	3.16
b/500	7.150	12.18	12.08	3.16	3.76	3.10
b/50	1.838	3.299	3.211	3.16	5.67	2.71
b/5	0.2787	0.6116	0.5564	2.24	7.56	1.45
b	0.0266	0.0913	0.0737			

1b. Points Located on Normal Through Reference Point

$\sigma_{zx} = \sigma_{xy} = 0$ (Symmetry)

(1) r	(2) σ_{xx}	(3) σ_{yy}	(4) σ_{zz}	(5) σ_{yz}	(6) (1)	(7) (2)	(8) (3)
b/500,000	174.41	145.19	436.63	-145.4	3.16	3.17	3.16
b/50,000	54.69	45.27	137.48	-46.16	3.16	3.22	3.16
b/5,000	16.82	13.71	42.79	-14.60	3.16	3.34	3.16
b/500	4.856	3.743	12.86	-4.624	3.16	3.77	3.15
b/50	1.113	0.6366	3.412	-1.485	3.16	7.01	2.97
b/5	0.0589	-.1906	0.4886	-.5296	2.24	-3.88	1.68
b	-.0139	-.1029	-.1255	-.2390			

(1) $(r_2/r_1)^{1/2}$ (2) $\sigma_{zz_1} / \sigma_{zz_2}$ (3) $(\sigma_{zz_1}-p)/(\sigma_{zz_2}-p)$

Table 2

Plane Strain Condition Close to the Tip of an Elliptical Crack

Stress distribution according to Chapter 3, 3.2.1.1.1, b = Minor halfaxis, r = Distance from reference point, intersection of minor axis with crack tip.
Major half axis a = 1.0 Minor half axis b = 0.5, pressure p = -1.0

Deviation in Percent from Plane Strain Condition (*)

r	(1) Δ_H%	(1) Δ_v%	(2) Δ_H%	(2) Δ_v%
b/500,000	0.06	0.08	0.181	0.25
b/50,000	0.18	0.25	0.56	0.79
b/5,000	0.57	0.77	1.78	2.49
b/500	1.76	2.51	5.65	8.03
b/50	5.89	8.37	18.4	26.6

Δ_H = Deviation at points located on the extension of the minor axis

Δ_v = Deviation at points located on the normal through the reference point

(1) Uniform pressure on the crack surfaces p = -1.0

(2) Uniform pressure on the crack surfaces p = -1.0 plus uniaxial tension t = -p parallel to the z axis

(*) Deviation of plane strain in x direction defined by:

$$\Delta = \frac{0.3\ (\sigma_{yy} + \sigma_{zz}) - \sigma_{xx}}{0.3(\sigma_{yy} + \sigma_{zz})}$$

Table 3

Comparison of Number of Net Polynomial Stress Functions, Generated by Displacement and Stress Field Formulation

Power i+j+k	(1) N	(2) N_E	Net Functions $N-N_E$	Power i+j+k	(1) N	(2) N_E	(3) $N_o=N-N_E$	(4) N_C	(5) N_{LC}	(6) N_{NC}	Net Functions $N=N_o-N_{NC}$
0	3	-	--								
1	9	-	6	0	6	0	6	0	0	0	6
2	18	3	15	1	18	3	15	0	0	0	15
3	30	9	21	2	36	9	27	6	0	6	21
4	45	18	27	3	60	18	42	18	3	15	27
5	63	30	33	4	90	30	60	36	9	27	33
6	84	45	39	5	126	45	81	60	18	42	39
7	108	63	45	6	168	63	105	90	30	60	45
8	135	84	51	7	216	84	132	126	45	81	51
9	165	108	57	8	270	108	162	168	63	105	57

(1) Number of linearly independent polynomials $c_j \cdot x^k \cdot y^m \cdot z^n$
(2) Number of polynomial functions which become linearly dependent by equilibrium requirement
(3) Number of linearly independent equilibrium stress functions
(4) Total number of compatibility equations
(5) Number of linearly dependent compatibility equations
(6) Number of linearly independent compatibility equations = Number of polynomial equilibrium stress functions which are linearly linked by compatibility requirement

Table 4

Comparison of the Net Number of Polynomial Stress Functions, Satisfying Equilibrium and Compatibility

Power i+j+k	(1) N	(2) N_r	(3) $N-N_r$	(4) $3\cdot(N-N_r)$	Desai
0	1	0	1	3	3
1	3	0	3	9	9
2	6	1	5	15	15
3	10	3	7	21	21
4	15	6	9	27	27
5	21	10	11	33	33
6	28	15	13	39	39
7	36	21	15	45	45
8	45	28	17	51	51

(1) Number of combinations of polynomials [26,27]

(2) Number of functions which become linearly dependent by requirement for homogeneous functions: $\nabla^2 \Phi = 0$

(3) Number of net harmonic polynomial functions

(4) Total number of linearly independent polynomial functions, based on Papkovitch-Neuber harmonic polynomial functions

Table 5

Resultant Stress Distribution on Model 1
(Fig. 7) Complete Interaction Power 2

Model Dimensions:
AX = 2.0 AY = 1.0 AZ = 5.0

Crack Size:
CX = 0.1 CY = 0.05

Location	S_{33}	S_{33}	S_{33}	S_{33}
1	0.0000	0.0000	0.0000	0.0000
2	0.0000	0.0000	0.0000	0.0000
3	0.0000	0.0000	0.0000	0.0000
4	0.0000	0.0000	0.0000	0.0000
5	0.0000	0.0000	0.0000	0.0000
6	0.0001	0.0001	0.0001	0.0001
7	0.0000	0.0000	0.0000	0.0000
8	1.0000	1.0000	1.0000	1.0000
9	1.0000	1.0000	1.0000	1.0000
10	0.0000	0.0000	0.0000	0.0000
11	0.0000	0.0000	0.0000	0.0000
WELCR	1.0	4000.0	10000.0	100000.0
α_1	1.000	1.000	1.000	1.000

WELCR = special weight of crack surface

α_1 = parameter of singular stress function

S_{33} = surface stress in normal direction

Table 6

Resultant Stress Distribution on Model 1
(Fig. 7) Complete Interaction Power 2

Model Dimensions:
AX = 2.0 AY = 1.0 AZ = 5.0

Crack Size:
CX = 0.25 CY = 0.125

Location	S_{33}	S_{33}	S_{33}
1	0.0000	0.0000	0.0000
2	0.0000	0.0000	0.0000
3	0.0000	0.0000	0.0000
4	0.0000	0.0000	0.0000
5	0.0000	0.0000	0.0000
6	0.0018	0.0018	0.0018
7	-0.0004	-0.0004	-0.0004
8	1.0000	1.0000	1.0000
9	0.9999	0.9999	1.0000
10	0.0002	0.0002	0.0002
11	0.0001	0.0001	0.0001
WELCR	1.0	720.0	720000.
α_1	1.000	1.000	1.000

WELCR = special weight of crack surface

α_1 = parameter of singular stress function

S_{33} = surface stress in normal direction

Table 7

Resultant Stress Distribution on Model 1
(Fig. 7) Complete Interaction Power 2

Model Dimensions:
AX = 2.0 AY = 1.0 AZ = 5.0

Crack Size:
CX=0.5 CY=0.25

Location	S_{33}	S_{33}	S_{33}	S_{33}
1	0.0006	0.0000	0.0000	0.0000
2	0.0005	0.0000	0.0000	0.0000
3	0.0006	0.0000	0.0000	0.0000
4	0.0006	0.0000	0.0000	0.0000
5	0.0006	0.0000	0.0000	0.0000
6	0.0141	0.0141	0.0141	0.0133
7	-0.0027	-0.0027	-0.0027	-0.0010
8	1.0002	1.0002	1.0001	0.9999
9	0.9996	0.9996	0.9996	1.0001
10	0.0017	0.0017	0.0017	0.0025
11	0.0005	0.0005	0.0005	-0.0011
WELCR	1.0	180.0	1800.0	2000000.0
α_1	1.003	1.003	1.003	1.002

WELCR = special weight of crack surface

α_1 = parameter of singular stress function

S_{33} = surface stress in normal direction

Table 8

Resultant Stress Distribution on Model 1
(Fig. 7) Complete Interaction Power 2

Model Dimensions:
AX = 2.0 Ay = 1.0 AZ = 5.0

Crack Size:
CX = 1.0 CY = 0.5

(*) Location	S_{33}	S_{33}	S_{33}	S_{33}
1	0.0082	0.0012	0.0004	0.0003
2	0.0064	-0.0007	-0.0013	-0.0011
3	0.0079	0.0009	0.0002	0.0001
4	0.0084	0.0014	0.0006	0.0004
5	0.0086	0.0015	0.0008	0.0006
6	0.1098	0.1106	0.1105	0.1092
7	-0.0186	-0.0187	-0.0184	-0.0161
8	0.9995	0.9995	0.9995	0.9990
9	0.9960	0.9960	0.9961	0.9969
10	0.0183	0.0184	0.0186	0.0197
11	0.0025	0.0025	0.0022	-0.0001
WELCR	1.0	10.0	100.0	1000.0
α_1	1.009	1.017	1.017	1.016

WELCR = special weight of crack surface, (multiplies)

α_1 = parameter of singular stress function

S_{33} = surface stress in normal direction

Table 9

Resultant Stress Distribution on Model 1
(Fig.7)

Complete interaction between singular and polynominal stress functions
Model dimensions and crack size corresponding to Table 5

Location (Fig. 7)	Power 2 S_{33}	Power 4 S_{33}
1	0.0000	-0.0008
2	0.0005	0.0006
3	0.0003	0.0008
4	0.0002	0.0004
5	0.0003	0.0005
6	0.1109	0.1313
7	-0.0196	0.0384
8	0.9965	0.9970
9	1.0021	0.9937
10	0.0201	0.0174
11	-0.0009	-0.0088
α_1	1.015	1.034

α_1 = Parameter of singular stress function

S_{33} = Surface stress in normal direction

Compatibility transformation of polynominal stress functions bypassed

WELCR = 40.0 even powers only

RESULT BY SHAH-KOBAYASHI[*]

$$\alpha_1 = 1.02 \pm 0.01$$

* The surface flaw ,ASME,NEW YORK,n.y.,1972 pp.111

Table 10

Resultant Stress Distribution on Model 2
Complete Interaction (Fig. 13)

Local surface effect neglected (Surface-crack treated as embedded)

Location (Fig. 12)	Power 2 S_{33}	Model Dimensions AX = 2.0 AY = 1.0 AZ = 5.0
1	0.0005	
2	-0.0000	Crack Dimensions
3	-0.0004	CX = 1.0 CY = 0.5
4	0.0005	
5	0.0005	
6	0.9988	Special Weight Factor on Crack Surface
7	1.0026	WELCR = 100.0
8	-0.0035	
9	0.0011	
10	0.0005	All Polynominal Stress Functions
11	16.9543	Compatible
12	-0.7072	
13	16.9543	
14	0.0046	
15	0.0082	
α_1	1.008	

Table 11

Resultant 3-Dimensional Stress Distribution in Model 5 (Fig. 14 and 15)

Model 5-1	σ_{xx}	σ_{yy}	σ_{zz}	σ_{yz}	σ_{zx}	σ_{xy}
1	0.002	0.315	-0.001	-0.001	-0.001	-0.003
2	0.001	0.328	-0.001	0.002	0.001	-0.001
3	0.002	0.344	-0.002	-0.001	0.001	0.005
4	-0.001	0.408	-0.001	-0.005	0.000	-0.037
5	-0.003	0.421	-0.001	-0.002	0.000	-0.004
6	-0.002	0.438	0.002	-0.005	-0.001	0.036
7	0.008	0.518	-0.003	0.001	-0.001	-0.060
8	0.004	0.579	-0.001	0.006	0.000	-0.002

Model 5-2	σ_{xx}	σ_{yy}	σ_{zz}	σ_{yz}	σ_{zx}	σ_{xy}
1	0.002	0.299	-0.001	-0.001	-0.006	-0.002
2	0.001	0.313	-0.001	0.002	0.000	-0.001
3	0.002	0.329	-0.002	-0.001	0.001	0.005
4	-0.001	0.394	-0.001	-0.005	0.000	-0.037
5	-0.003	0.407	-0.001	-0.002	0.000	-0.004
6	-0.002	0.424	0.002	-0.005	-0.000	-0.036
7	0.008	0.505	-0.003	0.001	-0.001	-0.060
8	0.004	0.566	-0.001	0.001	0.000	-0.002

Polynominal stress functions compatible power 2

WELCR - 1,000,000.0

Crack size 0.01117/0.01

Table 12

Resultant 3-Dimensional Stress Distribution in Model 3-1 and 3-8 (Fig. 16)

Model 3-1 is model 3-0 with single crack at 1

Model 3-1	σ_{xx}	σ_{yy}	σ_{zz}	σ_{yz}	σ_{zx}	σ_{xy}
1	0.007	0.001	0.001	-0.001	0.003	-0.003
2	0.005	0.001	-0.001	-0.000	0.004	-0.001
3	0.005	0.001	0.001	0.001	0.003	-0.001
4	0.003	0.001	-0.001	-0.001	-0.001	0.001
5	0.007	0.001	-0.001	0.000	-0.001	-0.001
6	0.013	0.000	0.001	0.001	-0.002	-0.006

Model 3-8	σ_{xx}	σ_{yy}	σ_{zz}	σ_{yz}	σ_{zx}	σ_{xy}
1	0.327	-0.000	0.048	-0.004	0.000	0.000
2	0.291	0.003	-0.016	-0.000	0.000	0.000
3	0.327	-0.000	0.048	0.004	0.000	0.000
4	0.327	-0.000	0.048	-0.004	0.000	0.000
5	0.291	0.003	-0.016	-0.000	0.000	0.000
6	0.327	-0.000	0.048	0.004	0.000	0.000
7	0.330	-0.054	0.108	-0.004	0.000	0.000
8	0.302	-0.032	0.038	-0.000	0.000	0.000

Polynominal stress functions compatible power 2

Weight on crack surfaces WELCR = 400,000.0

Crack size 0.01117/0.01

Table 13

Resultant Stress Distribution in Model 3 (Fig. 16)

Effect of higher power polynominal stress functions in symmetric model

Power 2	σ_{xx}	σ_{yy}	σ_{zz}	σ_{yz}	σ_{zx}	σ_{xy}
1	0.432	-0.000	0.039	-0.013	-0.114	0.074
2	0.373	-0.016	-0.029	-0.000	-0.114	0.000
3	0.432	-0.000	0.039	0.013	-0.114	-0.074
4	0.432	-0.000	0.039	-0.013	0.114	-0.074
5	0.373	-0.016	-0.029	-0.000	0.114	-0.000
6	0.432	-0.000	0.039	0.013	0.114	0.074

Power 4	σ_{xx}	σ_{yy}	σ_{zz}	σ_{yz}	σ_{zx}	σ_{xy}
1	0.466	0.000	0.010	0.000	-0.038	0.026
2	0.539	-0.007	0.014	0.000	-0.051	0.000
3	0.466	0.000	0.010	0.000	-0.038	-0.026
4	0.466	0.000	0.010	0.000	0.038	-0.026
5	0.539	-0.007	0.014	0.000	0.051	-0.000
6	0.466	0.000	0.010	0.000	0.038	0.026
7	0.702	0.003	-0.026	0.006	-0.052	0.085
8	1.061	-0.028	-0.033	0.000	0.000	0.000

Polynominal stress functions in equilibrium only

Odd sets of polynominal stress functions omitted

Table 14

Resultant 3-Dimensional Stress Distribution in Model 4 (Fig. 17)

Location	σ_{xx}	σ_{yy}	σ_{zz}	σ_{yz}	σ_{zx}	σ_{xy}
1	-0.005	0.014	0.600	0.000	0.000	0.000
2	-0.027	-0.002	0.582	0.000	0.000	0.000
3	-0.038	-0.010	0.572	0.000	0.000	0.000
4	0.021	0.004	0.608	0.000	0.000	0.002
5	-0.001	-0.012	0.590	0.000	0.000	0.001
6	-0.013	-0.020	0.580	0.000	0.000	0.001
7	0.004	-0.015	0.904	0.122	0.000	0.000
8	-0.018	-0.030	0.886	0.076	0.000	0.000
9	-0.030	-0.039	0.877	0.030	0.000	0.000
10	0.030	-0.025	0.912	0.122	-0.122	0.002
11	0.007	-0.040	0.894	0.076	-0.122	0.001
12	-0.004	-0.049	0.885	0.030	-0.122	0.001

Polynominal stress functions compatible power 2

Odd sets of polynominal stress functions omitted

No special functions

Table 15

Resultant 3-Dimensional Stress Distribution in Model 4 (Fig. 17)

Location	σ_{xx}	σ_{yy}	σ_{zz}	σ_{yz}	σ_{zx}	σ_{xy}
1	0.004	-0.109	0.640	0.000	0.000	0.000
2	0.014	-0.106	0.643	0.000	0.000	0.000
3	0.117	-0.158	1.026	0.000	0.000	0.000
4	0.020	-0.084	0.661	0.000	0.000	-0.004
5	0.029	-0.082	0.663	0.000	0.000	-0.002
6	0.133	-0.134	1.047	0.000	0.000	-0.001
7	-0.013	-0.081	0.865	0.077	0.000	0.000
8	-0.016	-0.155	0.903	0.027	0.000	0.000
9	-0.017	-0.204	0.933	0.005	0.000	0.000
10	0.003	-0.056	0.885	0.077	-0.088	-0.004
11	-0.000	-0.131	0.923	0.027	-0.088	-0.002
12	-0.002	-0.180	0.954	0.005	-0.088	-0.001

Polynominal stress functions compatible power 2

Odd sets of polynominal stress functions omitted

1 special stress function (closed form solution of cylindrican hole in infinite elastic body subjected to uniform tension with plane strain condition)

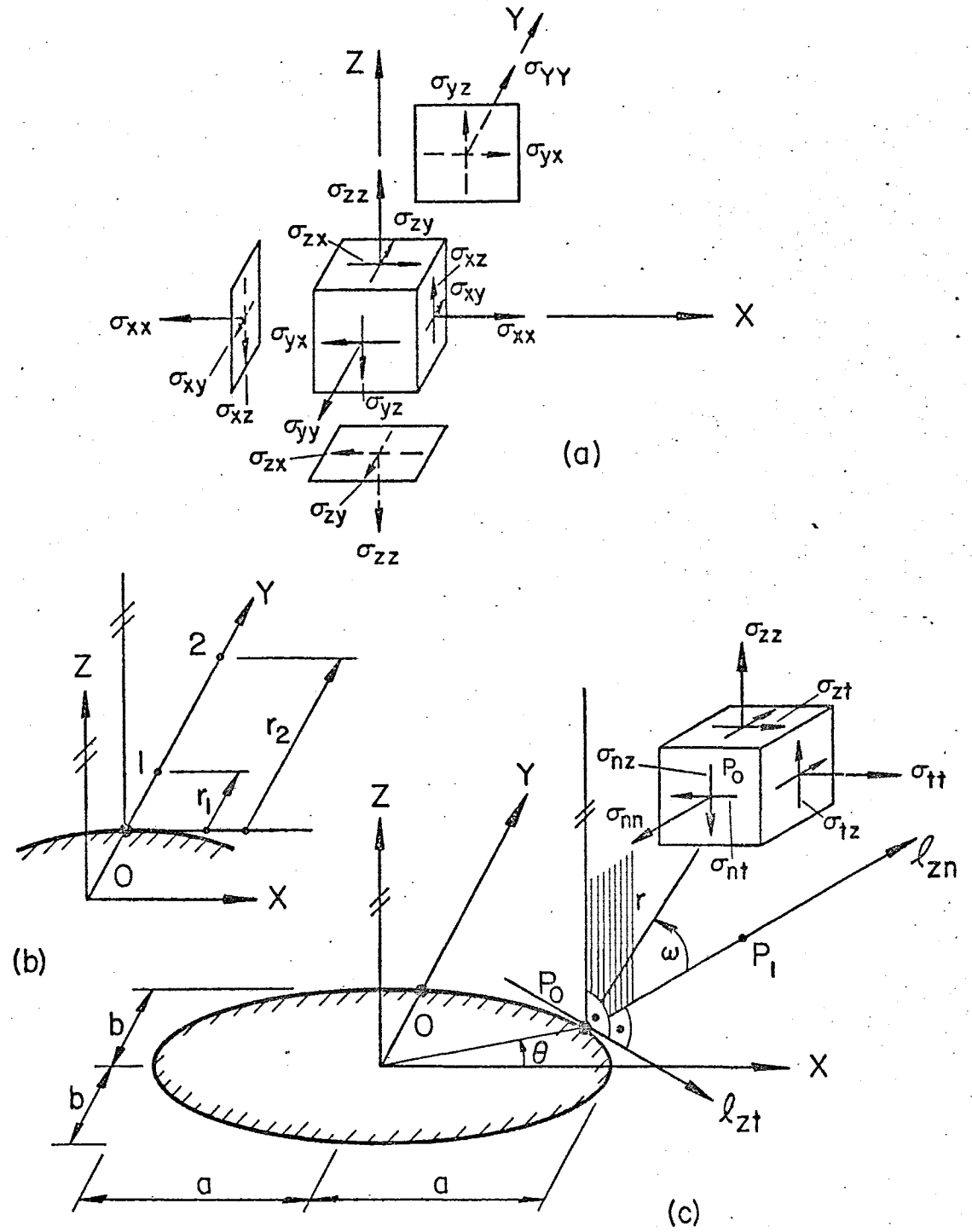

Fig. 1 Sign Convention and Rotation for Global Stresses and Stress Distribution Close to the Leading Edge of an Elliptical Crack

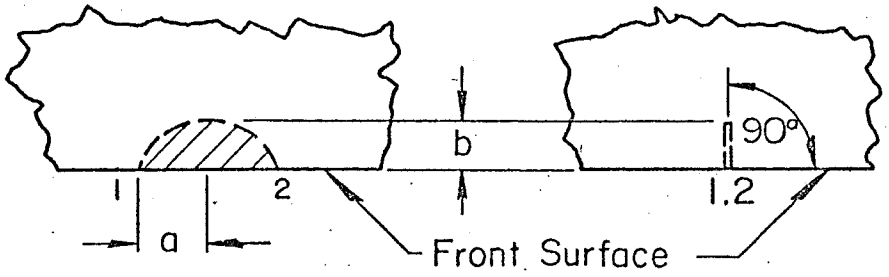

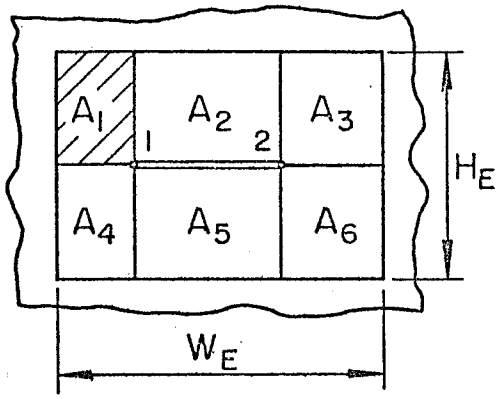

H_{E1} W_E = Effective Dimensions, Where Local Stresses, Due to Singular Stress Functions are Relevant

Consider Area A_1:

Love [3.6] Kobayashi [3.5]

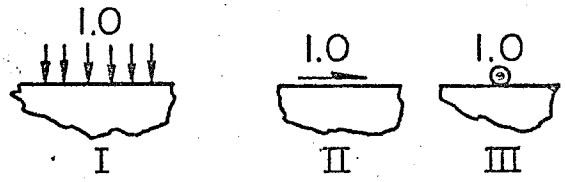

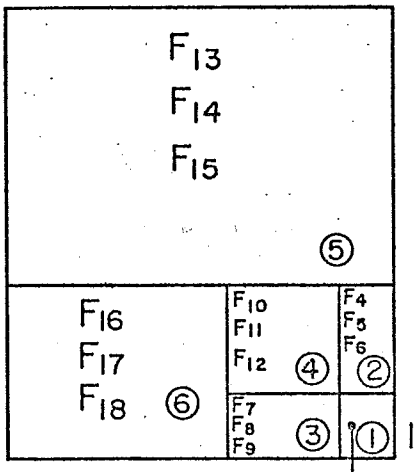

Area A_{21}, $\cdots$ A_4 are Treated Similar

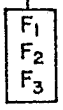

Subarea	Special Stress Function Associated with Loading		
	I	II	III
①	F_1	F_2	F_3
②	F_4	F_5	F_6
③	F_7	F_8	F_9
④	F_{10}	F_{11}	F_{12}
⑤	F_{13}	F_{14}	F_{15}
⑥	F_{16}	F_{17}	F_{18}

$F_1 \cdots F_{18}$ Functions, Defining 3 Dimensional Stress Distribution in Half Space, Due to Corresponding Load I, II, or III on Subareas ① $\cdots$ ⑤ [3.6, 3.5]

Fig. 2 Assignment of Special Nonsingular Stress Functions in a Surface Flaw Problem

$$\left\{ \begin{matrix} \bar{\alpha} \\ 0 \end{matrix} \right\} = \left[\bar{R} \right] \circ \left\{ \alpha \right\}$$

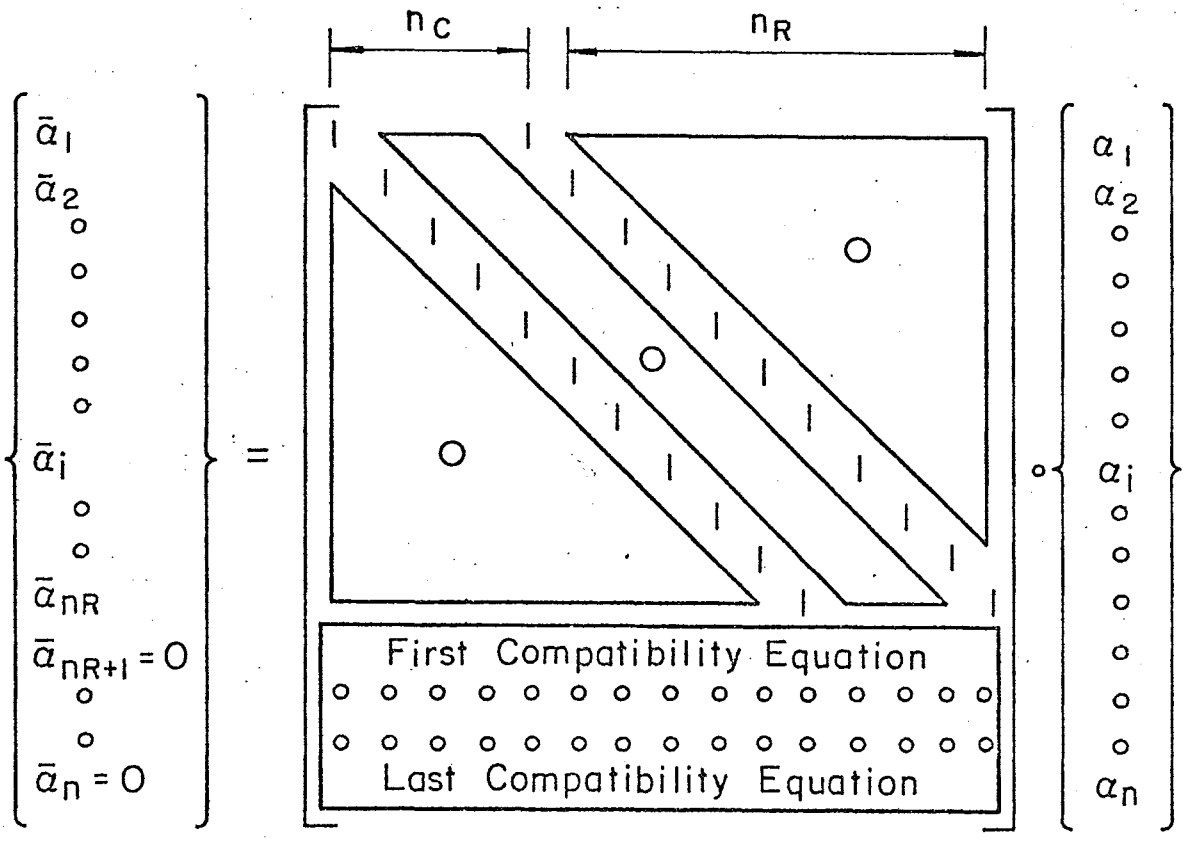

n = Total Number of Parameter α

n_R = Total Number of Reduced Parameters $\bar{\alpha}$

n_C = Number of Linearly Independent Compatibility Equations

Fig. 3 Compatibility Transformation Matrix $[\bar{R}]$ for Polynominal Stress Function Parameters

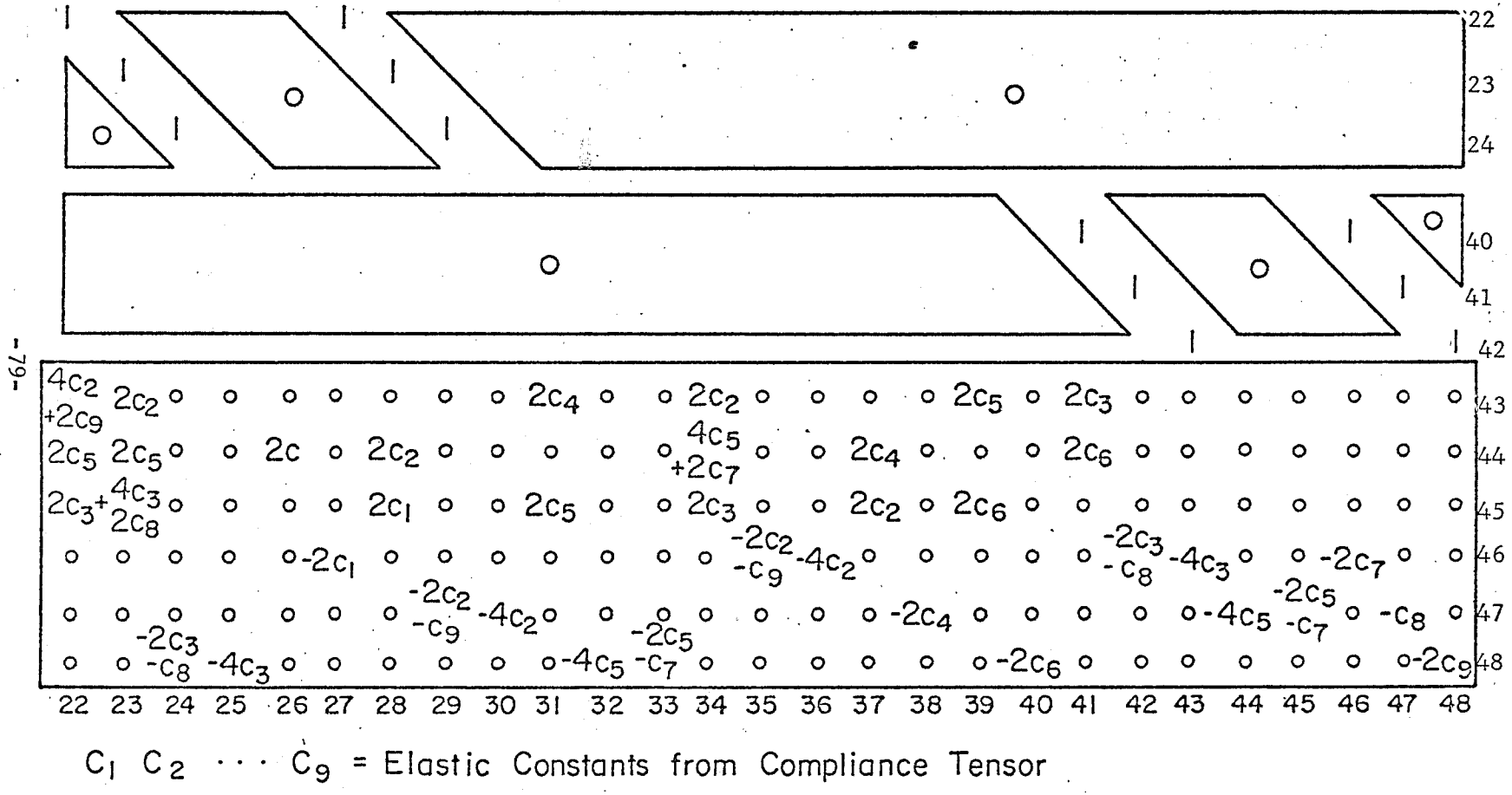

Fig. 4 Compatibility Transformation Matrix $[\bar{R}]$ for Second Power Set of Polynominal Stress Functions

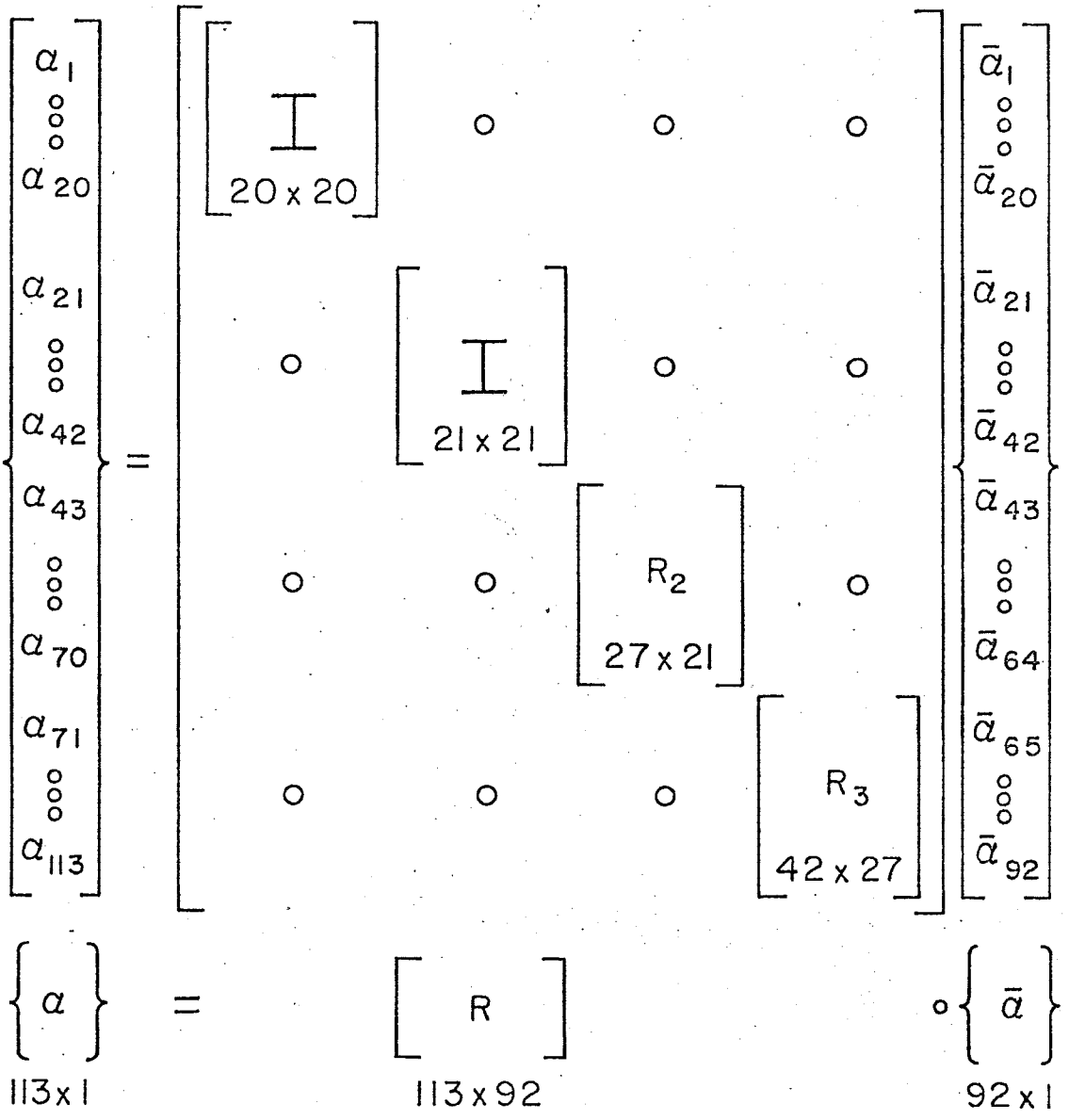

Fig. 5 Compatibility Transformation Matrix for Polynominal Stress Functions up to 3rd Power

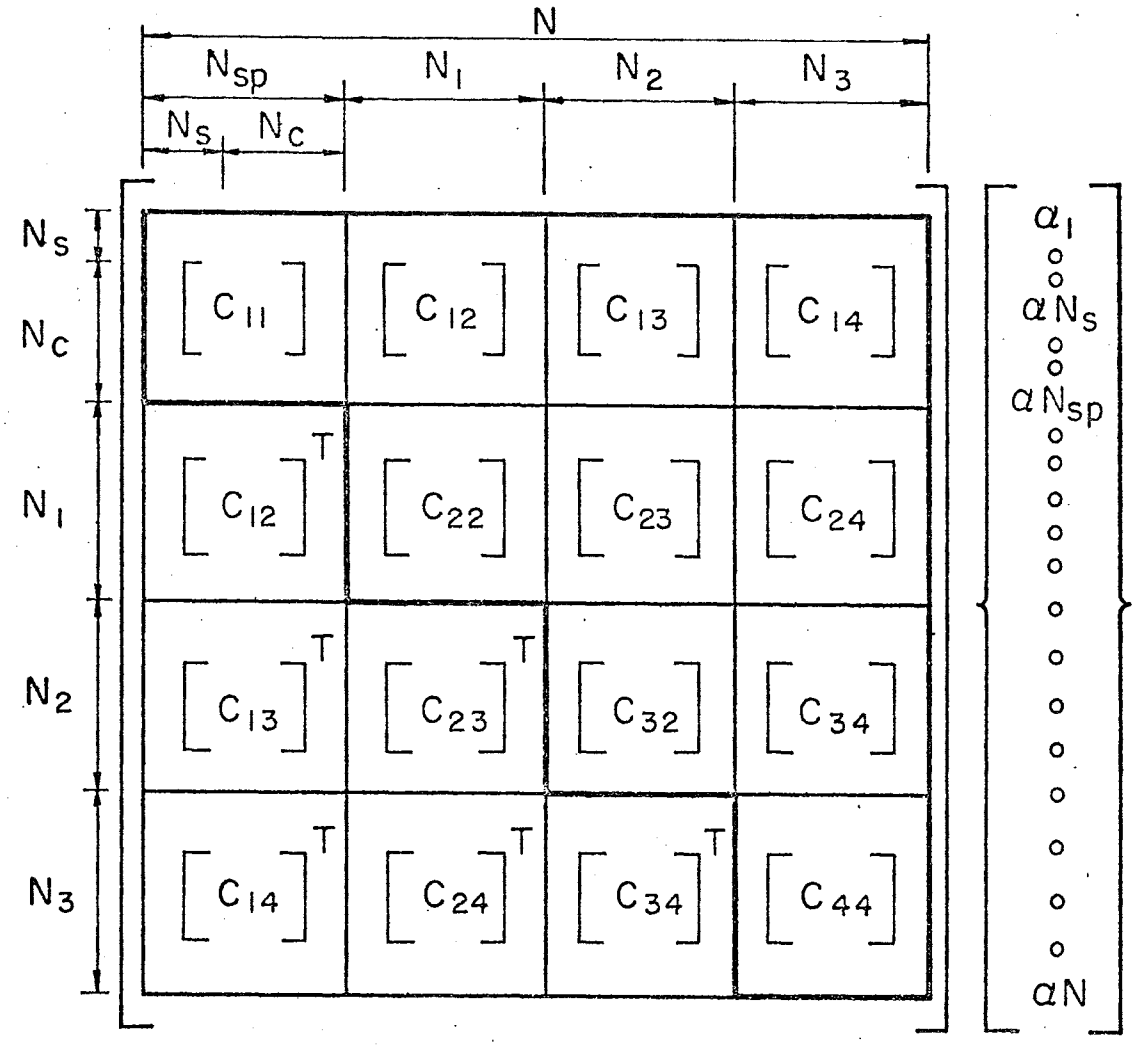

N_S = Number of Singular Stress Functions

Nd = Number of Classical Stress Functions

N_{sp} = Number of Special Special Stress Functions

N_1 = Number of P.S.F. of Power 0 and 1

N_2 = Number of P.S.F. of Power 2

N_3 = Number of P.S.F. of Power 3

N = Total Number of Stress Functions

$[C_{JK}]$ = Coefficient Submatrices

Fig. 6 Partitioned Original Coefficient Matrix

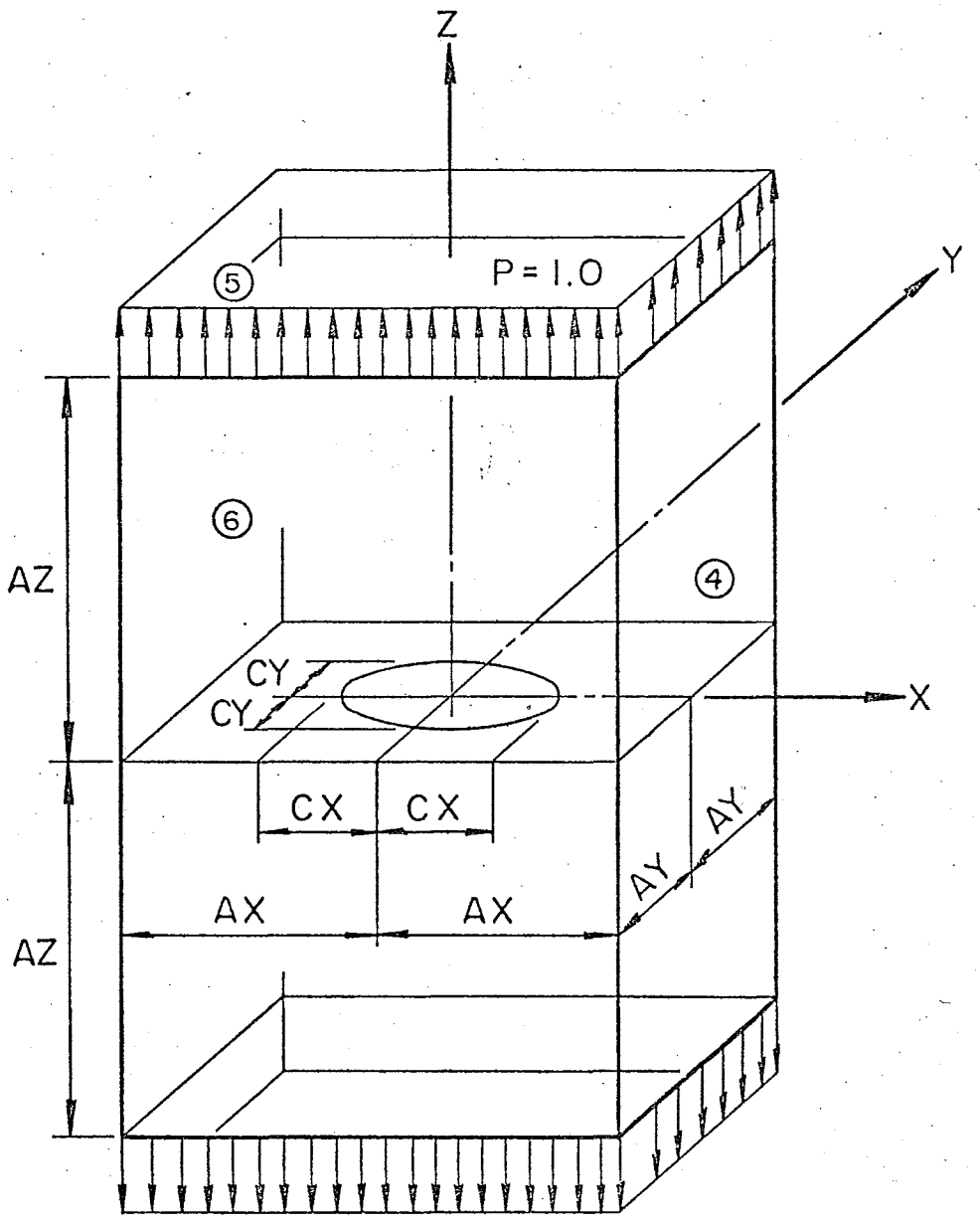

Fig. 7 Three Dimensional Solid (Hexahedron) with Embedded Elliptical Crack

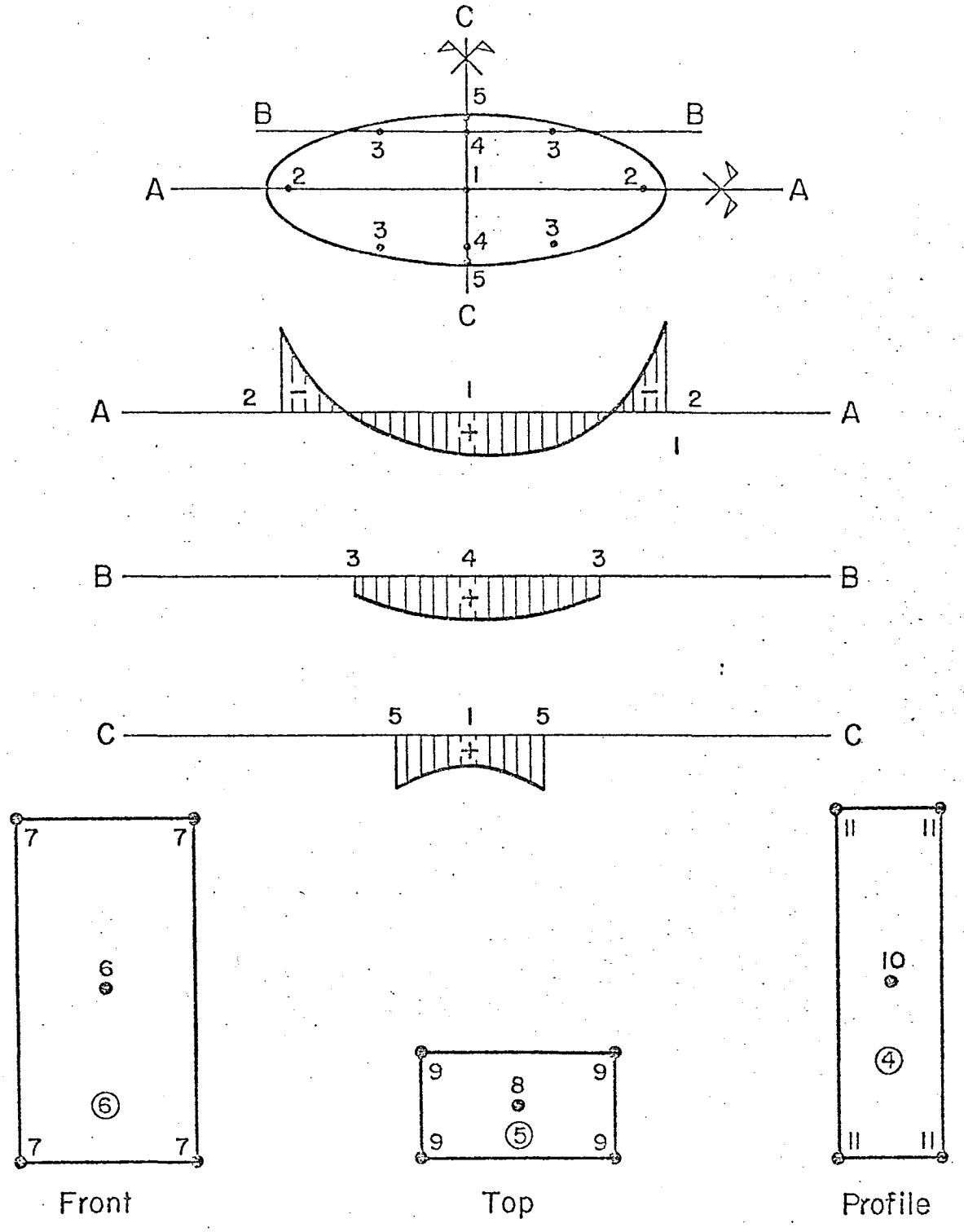

Fig. 8 Coordinates on Solid and Crack Surfaces and Schematic Stress Distribution on Model 1

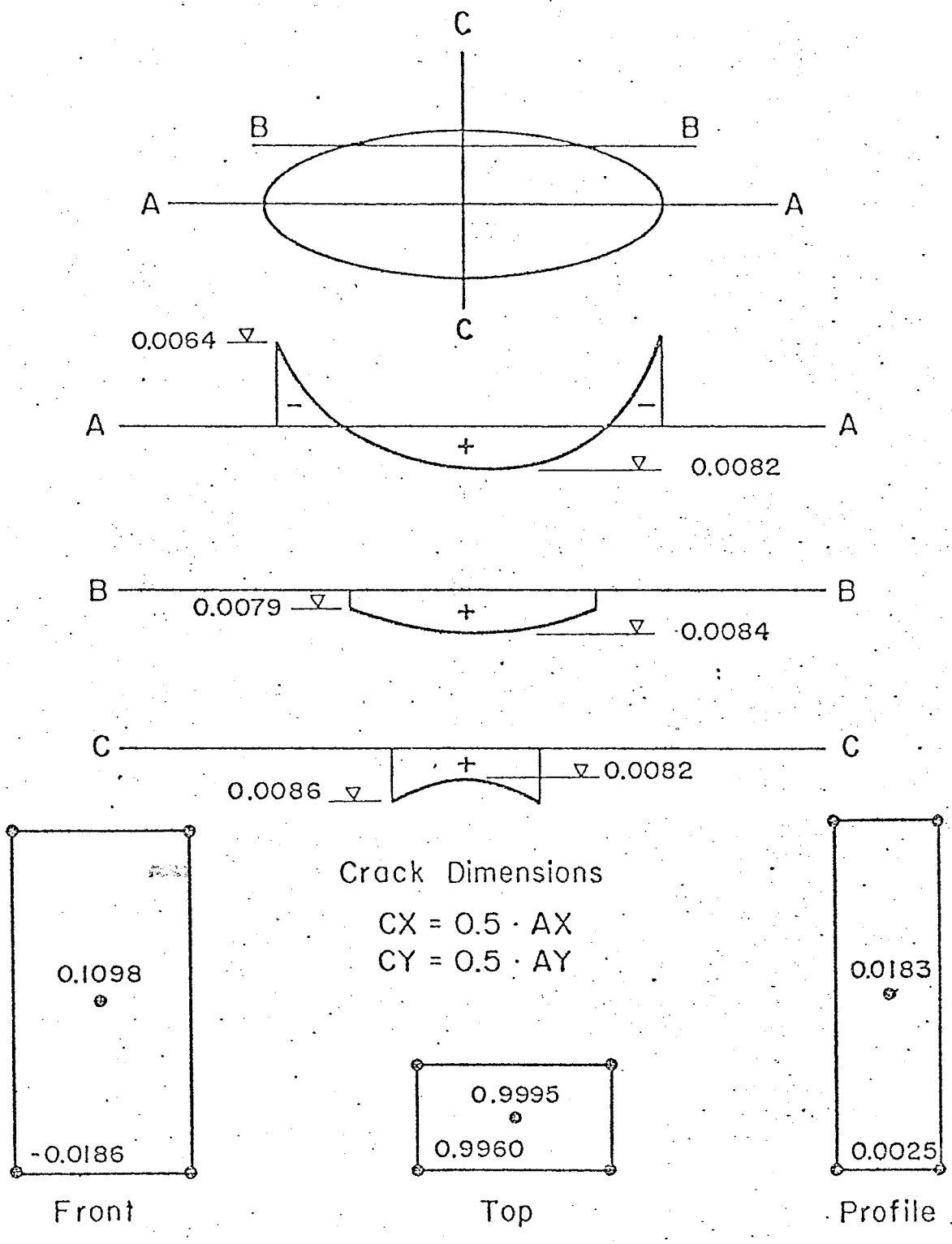

Fig. 9 Resultant Stress Distribution on Crack Surface and at Selected Points on the Solid Surface

Weight Factor = 1.0 Power 2

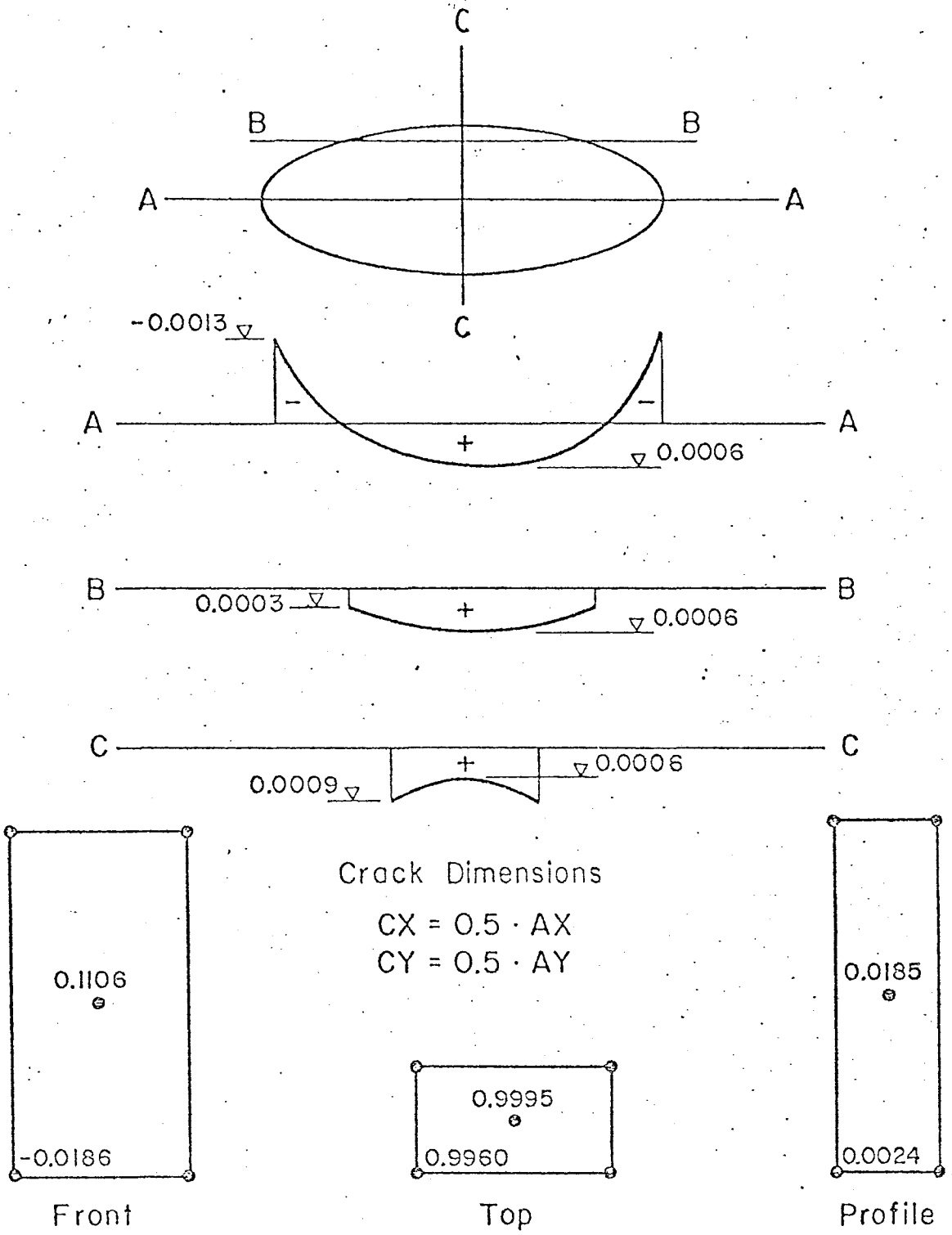

Fig. 10 Resultant Stress Distribution on Crack Surface and at Selected Points on the Solid Surface

Weight Factor = 40.0 Power 2

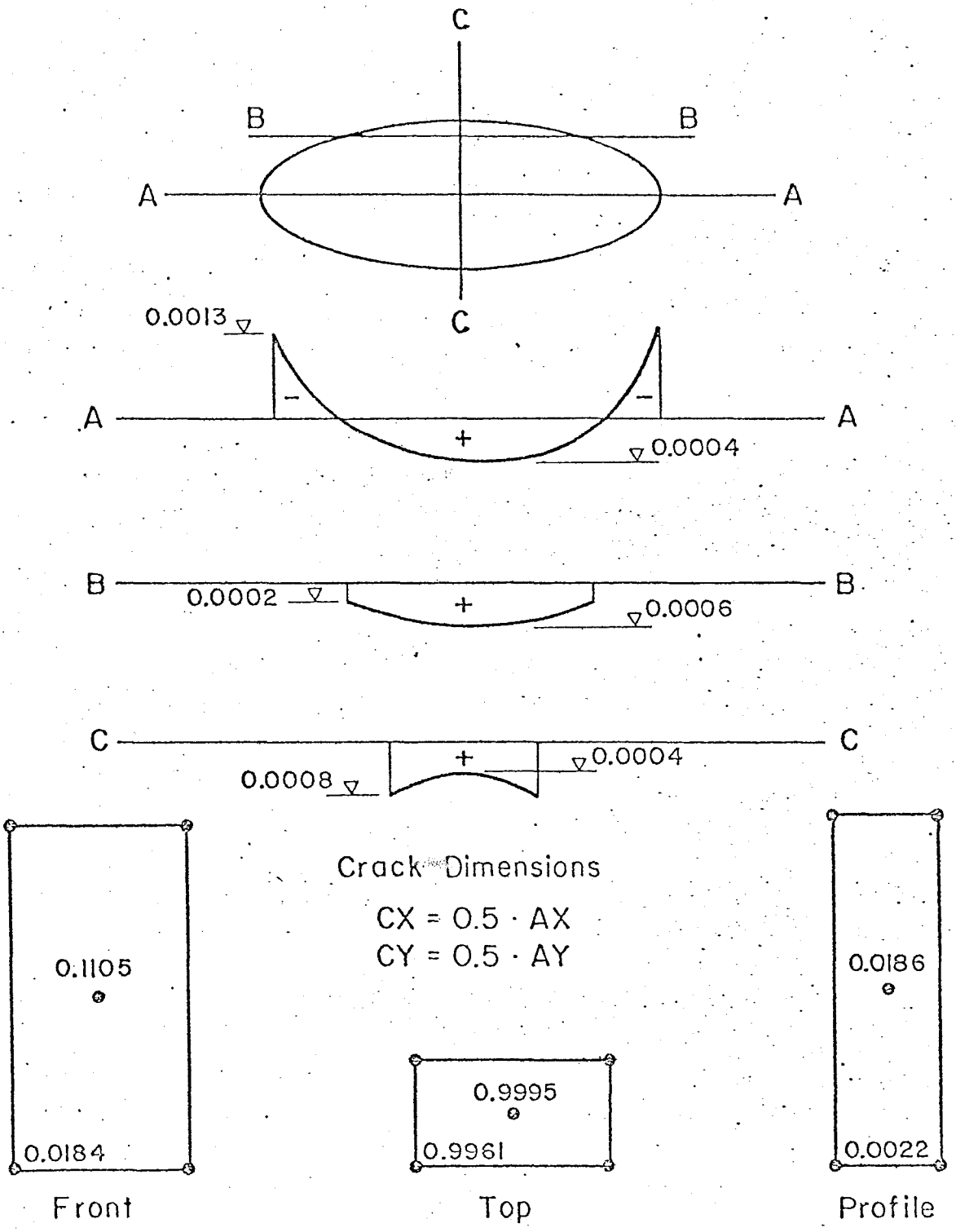

Fig. 11 Resultant Stress Distribution on Crack Surface and at Selected Points on the Solid Surface

Weight Factor = 100.0 Power 2

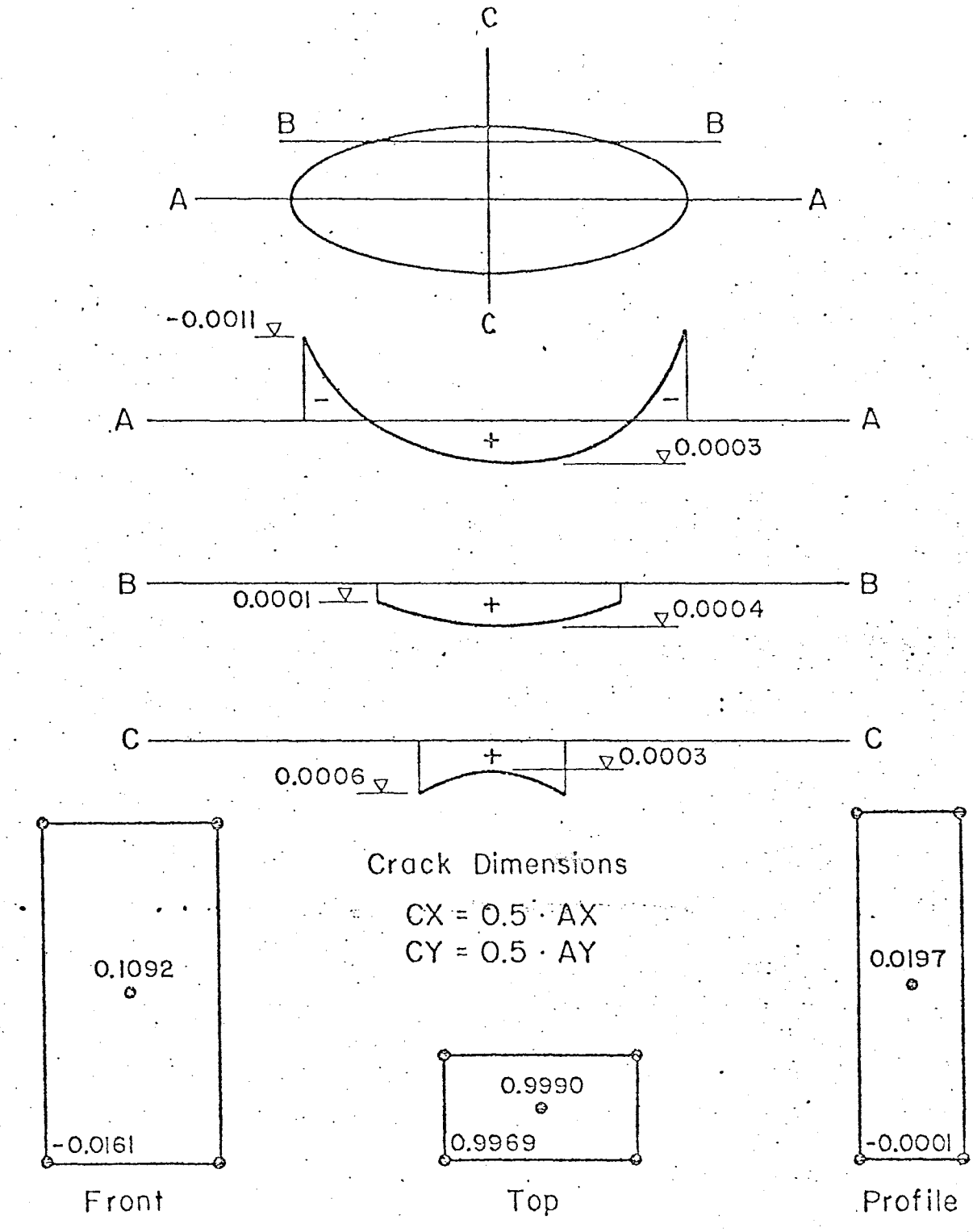

Fig. 12 Resultant Stress Distribution on Crack Surface and at Selected Points on the Solid Surface

Weight Factor = 1000.0 Power 3

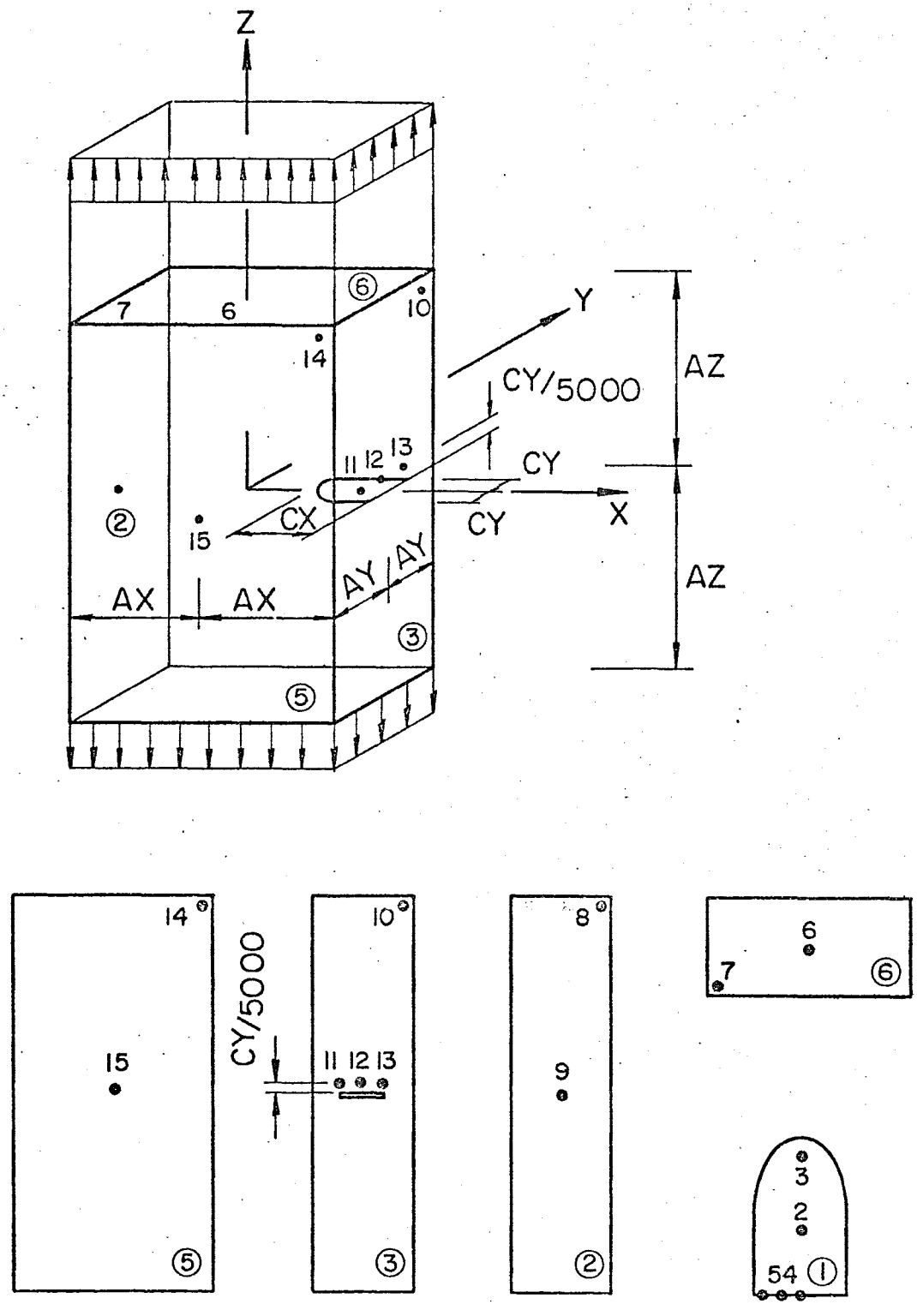

Fig. 13 Three Dimensional Solid with Semielliptical Crack (Embedded)

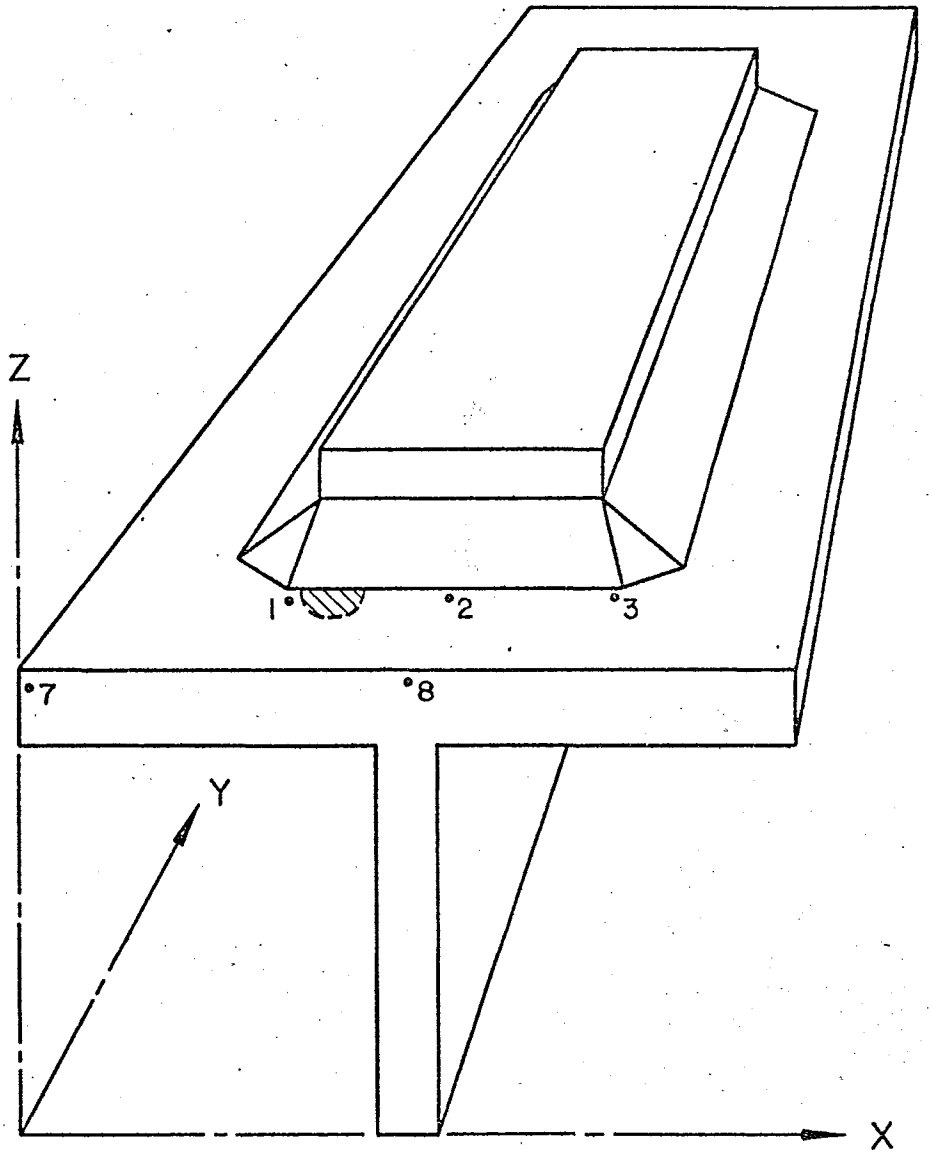

Fig. 14 Beam Flange with Welded Attachment

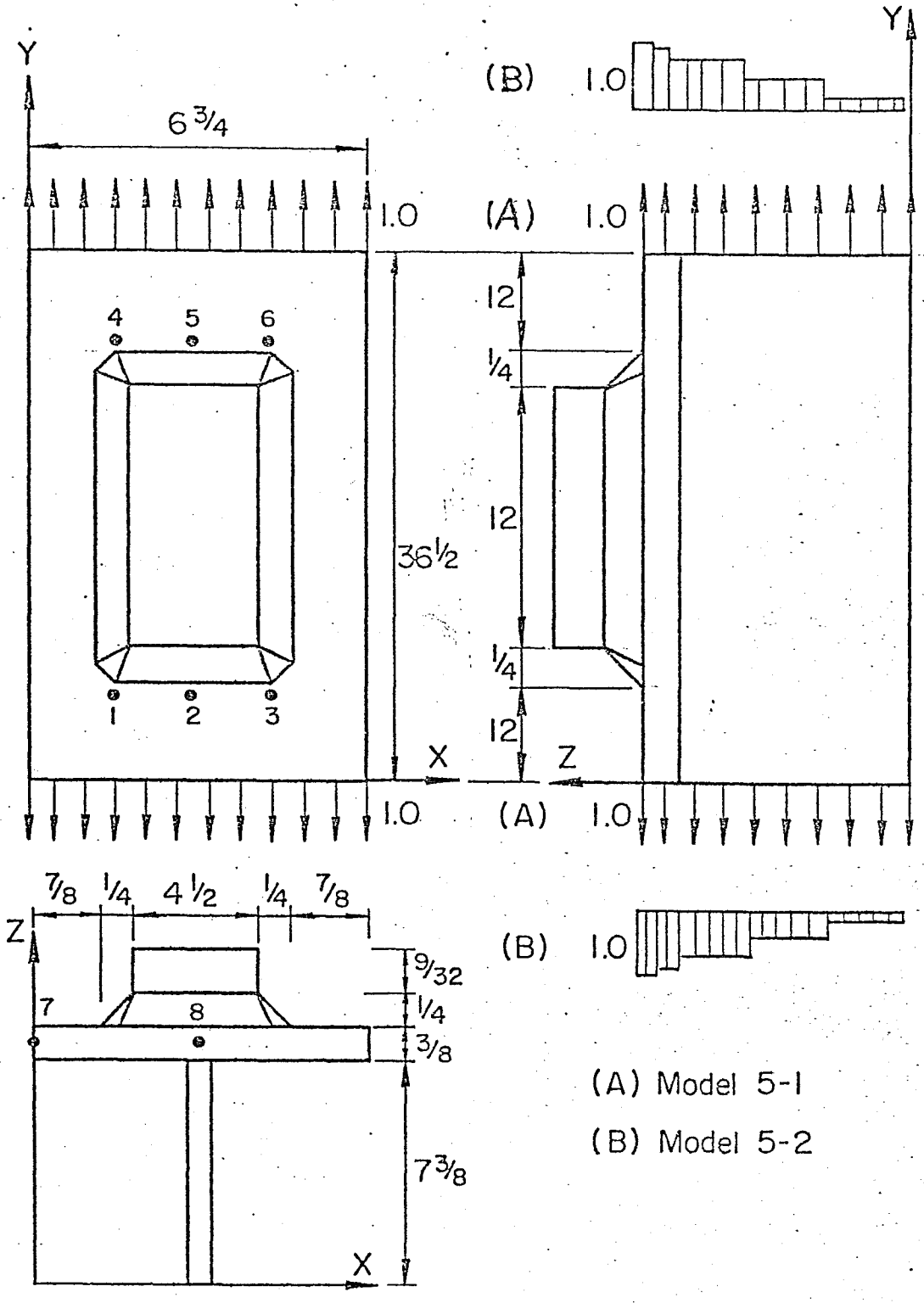

Fig. 15 Geometry of Beam Flange with Welded Attachment and Assumed Stress Distribution on Boundaries

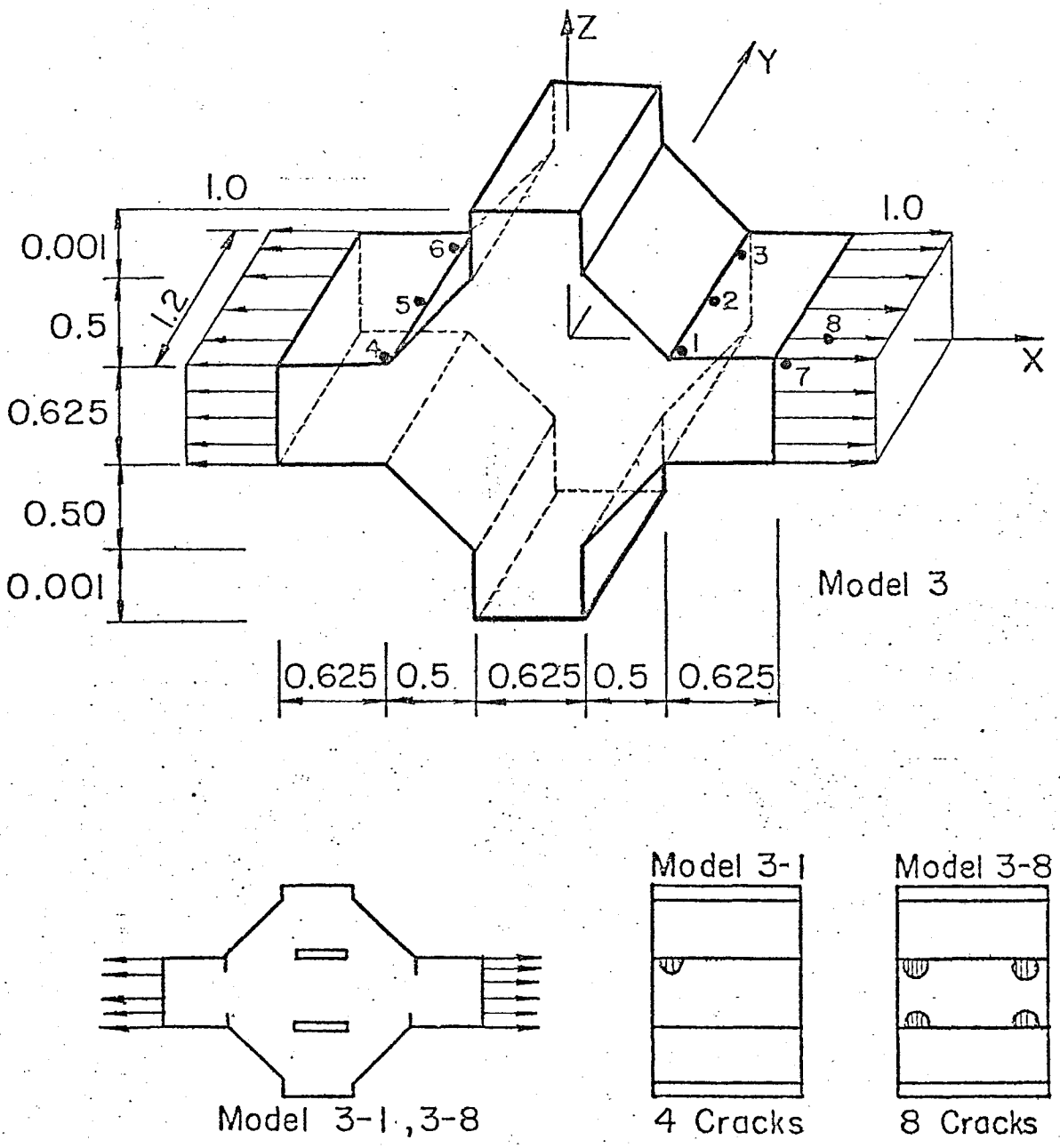

Fig. 16 Schematic of Three Dimensional Cruciform Joint

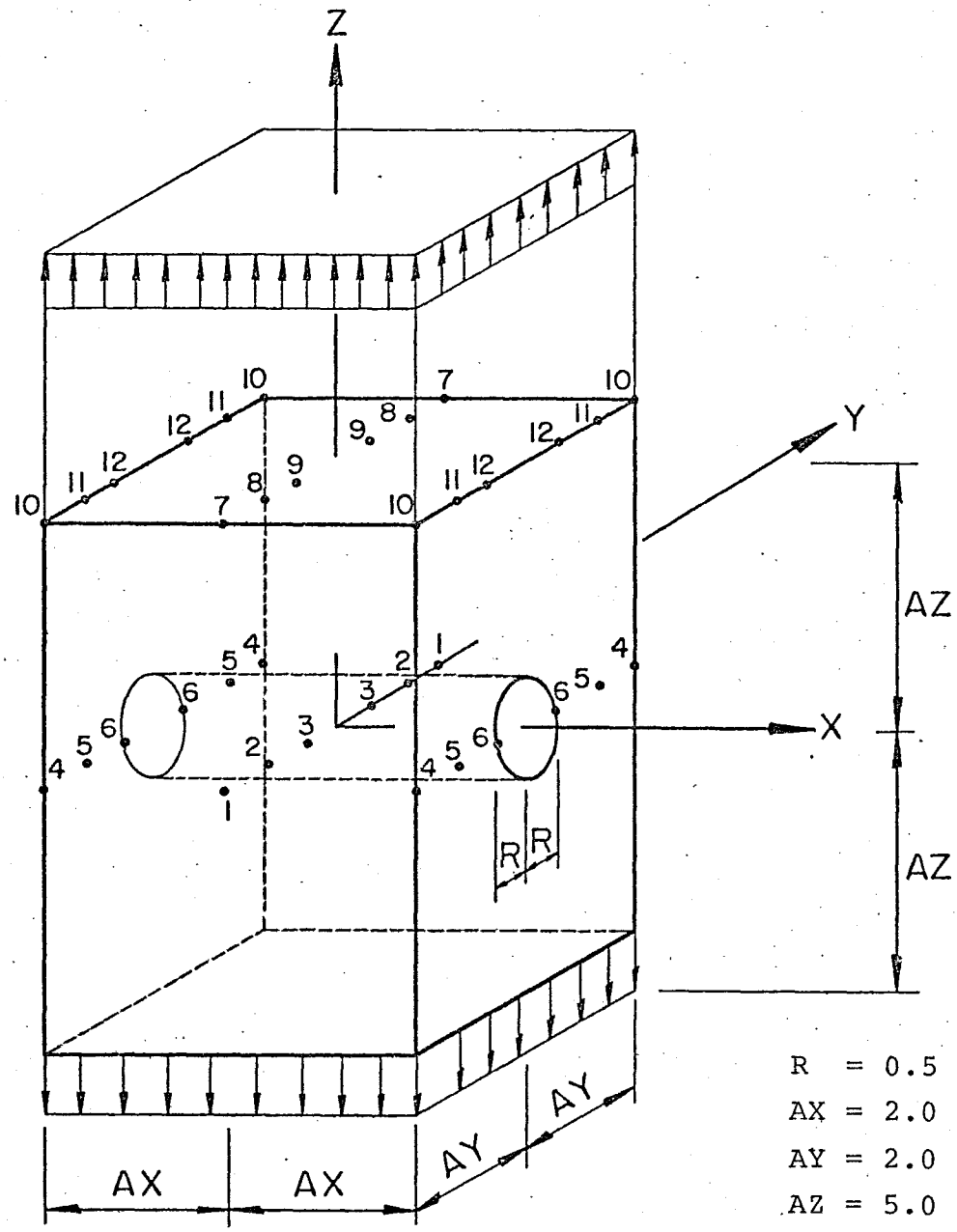

Fig. 17 Three Dimensional Solid with Cylindrical Hole

REFERENCES

1. Gran, R. J., Orazio, F. D., Paris, P. C., Irwin, G. R. and Hertzberg, R.
   INVESTIGATION AND ANALYSIS DEVELOPMENT OF EARLY LIFE AIRCRAFT STRUCTURAL FAILURES, AFFOL-TR-70-149

2. Barsom, J. M.
   FATIGUE CRACK GROWTH BEHAVIOR IN BRIDGE STEELS, Applied Research Laboratory, Monroeville, Pennsylvania, 1972

3. Fisher, J. W., Frank, K. H., Hirt, M. A., and McNamee, B. M.
   EFECT OF WELDMENTS ON THE FATIGUE STRENGTH OF STEEL BEAMS, NCHRP 102, Washington, D. C., 1970

4. Fisher, J. W., Albrecht, P., Yen, B. T., Klingerman, D. J. and McNamee, B. M.
   EFFECT OF WELDMENTS ON THE FATIGUE STRENGTH OF STEEL BEAMS-TRANSVERSE STIFFENERS AND ATTACHMENTS, Fritz Engineering Laboratory Report No. 334.10

5. Irwin, G. R.
   CHARACTERIZATION OF PART-THROUGH CRACKS IN TENSION, The Surface Crack, ASME, New York N. Y., 1972, pp. 1-10

6. Little, C. D. and Bunting, P. M.
   THE SURFACE FLAW IN AIRCRAFT STRUCTURES AND RELATED FRACTURE MECHANICS ANALYSIS, The Surface Crack, ASME, New York, N. Y., 1972, pp. 11-42

7. Kassir, M. K. and Sih, G. C.
   THREE DIMENSIONAL STRESS DISTRIBUTION AROUND AN ELLIPTICAL CRACK UNDER ARBITRARY LOADINGS, Journal of Applied Mechanics, September 1966, pp. 601-611

8. Irwin, G. R.
   THE CRACK EXTENSION FORCE FOR A PART-THROUGH CRACK IN A PLATE, Journal of Applied Mechanics, Vol. 29, Trans. ASME, Vol. 19, Series E, December 1962

9. Paris, P. C. and Sih, G. C.
STRESS ANALYSIS OF CRACKS, ASTM Stp. 381, 1970

10. Frank, K. H.
THE FATIGUE STRENGTH OF FILLET WELDED CONNECTIONS, Ph.D. Dissertation, Lehigh University, Bethlehem, Pennsylvania, 1971

11. Albrecht, P.
FATIGUE STRENGTH OF WELDED BEAMS WITH STIFFENERS, Ph.D. Dissertation, Lehigh University, Bethlehem, Pennsylvania, 1972

12. Marcal, P. V. and Bettis, R. S.
ELASTIC PLASTIC BEHAVIOR OF A LONGITUDINAL SEMI-ELLIPTICAL CRACK IN A THICK PRESSURE VESSEL, HEAVY SECTION STEEL TECHNOLOGY PROGRAM, 6th Annual Meeting, April 25-26, 1972, Paper 16,(ORNL)

13. Smith, F. W.
STRESS INTENSITY FACTORS FOR A SURFACE FRAMED FRACTURE SPECIMEN, NASA LERC Fracture Control Technology Review 25-26, January 1972

14. Kobayashi, A. S. and Shah, R. C.
STRESS INTENSITY FACTORS FOR AN ELLIPTICAL CRACK APPROACHING THE SURFACE OF A SEMI-INFINITE SOLID ENGINEERING FRACTURE MECHANICS, Engineering Fracture Mechanics, Vol. 2, No. 3, 1971

15. Desai, S.
USE OF AUXILIARY FUNCTIONS IN FINITE ELEMENT METHODS, Ph.D. Dissertation, Lehigh University, Bethlehem, Pennsylvania, 1971

16. Collatz, L.
THE NUMERICAL TREATMENT OF DIFFERENTIAL EQUATIONS, Springer Verlag, Berlin, 1960

17. Finlayson, B. A.
THE METHOD OF WEIGHTED RESIDUALS AND VARIATIONAL PRINCIPLES, Academic Press, New York, London, 1972

18. Green, A. E. and Sneddon, I. N.
THE DISTRIBUTION OF STRESS IN THE NEIGHBORHOOD OF A FLAT ELLIPTICAL CRACK IN AN ELASTIC SOLID, Proc. of Royal Society, London, England, Series A, Vol. 187, 1946, pp. 229-260

19. Irwin, G. R.
ANALYTICAL ASPECTS ON CRACK STRESS FIELD PROBLEMS, T. and A. M. Report No. 213, 1962, Theoretical and Applied Mechanics, University of Illinois

20. Kassir, M. K. and Sih, G. C.
THREE DIMENSIONAL STRESS DISTRIBUTION AROUND AN ELLIPTICAL CRACK UNDER ARBITRARY LOADINGS, Journal of Applied Mechanics, September 1966, pp. 601-611

21. Shah, R. C. and Kobayashi, A. S.
STRESS INTENSITY FACTOR FOR AN ELLIPTICAL CRACK UNDER ARBITRARY NORMAL LOADING, Engineering Fracture Mechanics, 1971, Vol. 3, pp. 71-96, Pergamon Press. Printed in Great Britain

22. Shah, R. C. and Kobayashi, A. S.
ON THE SURFACE FLAW PROBLEM, The Surface Crack, The American Society of Mechanical Engineers, New York, N. Y., November 26-30, 1972, pp. 87-89

23. Love, A. E. H.
THE STRESS PRODUCED IN A SEMI-INFINITE SOLID BY PRESSURE ON PART OF THE BOUNDARY, Phil. Trans. Royal Society (A), Vol. 228 (1929), pp. 377-420

24. Westergard, H. M.
THEORY OF ELASTICITY AND PLASTICITY, Dover Publications Inc., New York, N. Y., pp. 142-148

25. Sadowsky, M. A. and Sternberg, E.
STRESS CONCENTRATION AROUND AN ELLIPSOIDAL CAVITY IN AN INFINITE BODY UNDER ARBITRARY PLANE STRESS PERPENDICULAR TO THE AXIS OF REVOLUTION OF CAVITY, Journal of Applied Mechanics, September 1947, pp. A191-A201

26. Desai, S.
THREE DIMENSIONAL POLYNOMIAL STRESS FUNCTIONS (in preparation)

27. Timoshenko and Coodier
THEORY OF ELASTICITY, P. 242, Text McGraw-Hill, Third Edition, New York

28. Rivlin, T. J.
AN INTRODUCTION TO APPROXIMATION OF FUNCTIONS, Blaisdell Publishing Company, Waltham, Massachusetts, 1969

29. Lekhnitskii, S. G.
THEORY OF ELASTICITY OF AN ANISOTROPIC ELASTIC BODY, Holden-Day, Inc., San Francisco, 1963

30. Worch, G.
ELASTISCHE SCHEIBEN, Beton Kalender 1967, Wilhelm Ernst & Sohn, Berlin, p. 51

31. Hartranft, R. J. and Sih, G. C.
ALTERNATING METHOD APPLIED TO EDGE AND SURFACE CRACK PROBLEMS, Technical Report NASA-TR-72-1, April 1972

APPENDIX A1

EXTERIOR GALERKIN METHOD

Substitution of $S = \sum_{i=1}^{3} s_i \alpha_i$

into Eq. (6b) yields

$$\begin{aligned}
&\int_b [s_1\alpha_1+s_2\alpha_2+s_3\alpha_3-t]s_1\cdot\alpha_1 \, da = 0 \\
&\int_b [s_1\alpha_1+s_2\alpha_2+s_3\alpha_3-t]s_2\cdot\alpha_2 \, da = 0 \qquad \text{(A.1)} \\
&\int_b [s_1\alpha_1+s_2\alpha_2+s_3\alpha_3-t]s_3\cdot\alpha_3 \, da = 0
\end{aligned}$$

LEAST SQUARE METHOD

Minimization of the functional $(s-t)^2$ yields

$$\int_b \frac{\partial}{\partial\alpha_{1,2,2}}[s_1\alpha_1+s_2\alpha_2+s_3\alpha_3-t][s_1\alpha_1+s_2\alpha_2+s_3\alpha_3-t]da = 0$$

$$\begin{aligned}
&2\cdot\int_b [s_1\alpha_1+s_2\alpha_2+s_3\alpha_3-t]\cdot s_1 \, da = 0 \\
&2\cdot\int_b [s_1\alpha_1+s_2\alpha_2+s_3\alpha_3-t]\cdot s_2 \, da = 0 \qquad \text{(A.2)} \\
&2\cdot\int_b [s_1\alpha_1+s_2\alpha_2+s_3\alpha_3-t]\cdot s_3 \, da = 0
\end{aligned}$$

System Eq. (A.1) and system Eq. (A.2) are actually identical, since both can be modified to Eq. (A.3) since, in general $\alpha_1 \neq 0$, $\alpha_2 \neq 0$, $\alpha_3 \neq 0$, and $2 \neq 0$

$$\int_b [s_1\alpha_1+s_2\alpha_2+s_3\alpha_3-t]s_1 \, da = 0$$

$$\int_b [s_1\alpha_1+s_2\alpha_2+s_3\alpha_3-t]s_2 \, da = 0 \qquad \text{(A.3)}$$

$$\int_b [s_1\alpha_1+s_2\alpha_2+s_3\alpha_3-t]s_3 \, da = 0$$

APPENDIX A2

POLYNOMINAL STRESS FUNCTIONS, SATISFYING EQUILIBRIUM ZERO AND FIRST POWER

σ	α_1	α_2	α_3	α_4	α_5
xx	1.0	-	-	-	-
yy	-	1.0	-	-	-
zz	-	-	1.0	-	-
yz	-	-	-	1.0	-
zx	-	-	-	-	1.0
xy	-	-	-	-	-

σ	α_6	α_7	α_8	α_9	α_{10}
xx	-	x	x	y	z
yy	-	-	-	-	-
xx	-	-	-	-	-
yz	-	-	-	-	-
zx	-	-	-z	-	-
xy	1.0	-y	-	-	-

σ	α_{11}	α_{12}	α_{13}	α_{14}	α_{15}
xx	-	-	-	-	-
yy	x	y	y	z	-
zz	-	-	-	-	x
yz	-	-	-z	-	-
zx	-	-	-	-	-
xy	-	-x	-	-	-

σ	α_{16}	α_{17}	α_{18}	α_{19}	α_{20}
xx	-	-	-	-	-
yy	-	-	-	-	-
zz	y	z	z	-	-

yz	-	-	-y	x	-
zx	-	-x	-	-	y
xy	-	-	-	-	-

σ	α_{21}
xx	-
yy	-
zz	-
yz	-
zx	-
xy	z

SECOND POWER

σ	α_{22}	α_{23}	α_{24}	α_{25}	α_{26}
xx	x^2	x^2	xy	2xy	y^2
yy	y^2	-	-	-	-
zz	-	z^2	-	-	-
yz	-	-	-	-	-
zx	-	-2xz	-yz	-	-
xy	-2xy	-	-	$-y^2$	-

σ	α_{27}	α_{28}	α_{29}	α_{30}	α_{31}
xx	yz	z^2	zx	2zx	-
yy	-	-	-	-	x^2
zz	-	-	-	-	-
yz	-	-	-	-	-
zx	-	-	-	$-z^2$	-
xy	-	-	-yz	-	-

σ	α_{32}	α_{33}	α_{34}	α_{35}	α_{36}
xx	-	-	-	-	-
yy	2xy	xy	y^2	yz	2yz
zz	-	-	z^2	-	-
yz	-	-xy	-2yz	-	$-z^2$
zx	$-x^2$	-	-	-zx	-

σ	α_{37}	α_{38}	α_{39}	α_{40}	α_{41}
xx	-	-	-	-	-
yy	z^2	zx	-	-	-
zz	-	-	x^2	xy	y^2
zy	-	-	-	-	-
zx	-	-	-	-	-
xy	-	-	-	-	-

σ	α_{42}	α_{43}	α_{44}	α_{45}	α_{46}
xx	-	-	-	-	-
yy	-	-	-	-	-
zz	yz	2yz	2zx	zx	-
yz	-	$-y^2$	-	-xy	x^2
zx	-yx	-	$-x^2$	-	-
xy	-	-	-	-	-

σ	α_{47}	α_{48}
xx	-	-
yy	-	-
zz	-	-
yz	-	-
zx	y^2	-
xy	-	z^2

APPENDIX A3

COMPATIBILITY EQUATIONS FOR HOMOGENEOUS ORTHOTROPIC MATERIALS

Defining the stress-strain relationship for linear elastic materials as:

$$\{\sigma\} = [D] \cdot \{\varepsilon\}$$

the compliance tensor [D] for homogeneous materials is defined in Ref. (29) as:

Isotropic Material

$$\begin{bmatrix} c_1 & c_2 & c_2 & 0 & 0 & 0 \\ c_2 & c_1 & c_2 & 0 & 0 & 0 \\ c_2 & c_2 & c_1 & 0 & 0 & 0 \\ 0 & 0 & 0 & c_3 & 0 & 0 \\ 0 & 0 & 0 & 0 & c_3 & 0 \\ 0 & 0 & 0 & 0 & 0 & c_3 \end{bmatrix}$$

Orthotropic Material

$$\begin{bmatrix} c_1 & c_2 & c_3 & 0 & 0 & 0 \\ c_2 & c_4 & c_5 & 0 & 0 & 0 \\ c_3 & c_5 & c_6 & 0 & 0 & 0 \\ 0 & 0 & 0 & c_7 & 0 & 0 \\ 0 & 0 & 0 & 0 & c_8 & 0 \\ 0 & 0 & 0 & 0 & 0 & c_9 \end{bmatrix}$$

where $c_1 = E$

$c_2 = \nu \cdot E$

$c_3 = \frac{E}{2(1+\nu)} = G$

$G = \mu$

c_1 through c_9 arbitrary

Substituting the strain-stress relationship into the compatibility equations, the following set of 6 equations can be obtained:

Compatibility Equations in Terms of Stresses:

$$c_1\cdot\sigma_{xx,yy}+c_2(\sigma_{yy,yy}+\sigma_{xx,xx})+c_3\sigma_{zz,yy}$$
$$+c_4\cdot\sigma_{yy,xx}+c_5\cdot\sigma_{zz,xx}-c_9\sigma_{xy,xy} = 0 \qquad (A.4)$$

$$c_2\sigma_{xx,zz}+c_3\cdot\sigma_{xx,yy}+c_4\sigma_{yy,zz}+$$
$$c_5(\sigma_{yy,yy}+\sigma_{zz,zz})+c_6\sigma_{zz,yy}-c_7\sigma_{yz,yz} = 0 \qquad (A.5)$$

$$c_1\sigma_{xx,zz}+c_2\sigma_{yy,zz}+c_3(\sigma_{xx,xx}+\sigma_{zz,zz})$$
$$+c_5\sigma_{yy,xx}+c_6\sigma_{zz,xx}-c_8\sigma_{zx,zx} = 0 \qquad (A.6)$$

$$-2c_1\sigma_{xx,yz}-2c_2\sigma_{yy,yz}-2c_3\sigma_{zz,yz}-c_7\sigma_{yz,xx}$$
$$+c_8\sigma_{zx,xy}+c_9\sigma_{xy,zx} = 0 \qquad (A.7)$$

$$-2c_2\sigma_{xx,zx}-2c_4\sigma_{yy,zx}-2c_5\sigma_{zz,zx}+$$
$$c_7\sigma_{yz,xy}-c_8\sigma_{zx,yy}+c_9\sigma_{xy,yz} = 0 \qquad (A.8)$$

$$-2c_3\sigma_{xx,xy}-2c_5\sigma_{yy,xy}-2c_6\sigma_{zz,xy}$$
$$+c_7\sigma_{yz,zx}+c_8\sigma_{zx,yz}-c_9\sigma_{xy,zz} = 0 \qquad (A.9)$$

Compatibility Equations for 2nd Power Polynominal Stress Functions (Homogeneous Expressions)

$$c_1\cdot(2\alpha_{26})+c_2(4\alpha_{22}+2\ _{23}+2\alpha_{34})+c_3(2\alpha_{41})$$
$$+c_4(2\alpha_{31})+c_5(2\alpha_{39})+c_9(2\alpha_{22}) = 0 \qquad (A.10)$$

$$c_2(2\alpha_{28})+c_3(2\alpha_{26})+c_4(2\alpha_{37})+c_5(2\alpha_{22}+$$
$$2\alpha_{23}+4\alpha_{34})+c_6(2\alpha_{41})+c_7(2\alpha_{34}) = 0 \qquad (A.11)$$

$$c_1(2\alpha_{28})+c_3(2\alpha_{37})+c_4(2\alpha_{22}+4\alpha_{23}+2\alpha_{34})$$
$$+c_5(2\alpha_{31})+c_6(2\alpha_{39})+c_8(2\alpha_{23}) = 0 \qquad (A.12)$$

$$c_1(-2\alpha_{27})+c_2(-2\alpha_{35}-4\alpha_{36})+c_3(-2\alpha_{42}-4\alpha_{43})$$
$$+c_7(-2\alpha_{46})+c_8(-\alpha_{42})+c_5(-\alpha_{35}) = 0 \qquad (A.13)$$

$$c_2(-2\alpha_{29}-4\alpha_{30})+c_4(-2\alpha_{38})+c_5(-4\alpha_{44}-2\alpha_{45})$$
$$+c_7(-\alpha_{45}) = c_8(-\alpha_{47})+c_9(-\alpha_{29}) = 0 \qquad (A.14)$$

$$c_3(-2\alpha_{24}-4\alpha_{25})+c_5(-4\alpha_{32}-2\alpha_{33})+c_6(-2\alpha_{40})$$
$$+c_7(-\alpha_{33})+c_8(-\alpha_{24})+c_8(-\alpha_{48}) = 0 \qquad (A.15)$$

These equations (A.10) through (A.15) are substituted into rows 43 through 48 in Fig. 4.

APPENDIX A4

Stress Distribution Near the Leading Edge of an Elliptical Crack

The stress distribution near the leading edge of an elliptical crack can be derived from the general solution given by Kassir and Sih.[20]

For the case of uniform pressure acting on the crack surfaces equations 40a through 40f in Ref. 20 p. 608 can be reduced to the following set of equations when $\omega = \theta$.

$$K_{II} = K_{III} = 0 \text{ and } K_I = (\pi)^{1/2} k_1$$

$$\sigma_{nn} = \frac{K_I}{(2\pi r)^{1/2}} \cos \frac{\omega}{2} \left(1 - \sin \frac{\omega}{2} \sin \frac{3\omega}{2}\right) \qquad (A.16)$$

$$\sigma_{zz} = \frac{K_I}{(2\pi r)^{1/2}} \cos \frac{\omega}{2} \left(1 + \sin \frac{\omega}{2} \sin \frac{3\omega}{2}\right) \qquad (A.17)$$

$$\sigma_{tt} = \frac{K_I}{(2\pi r)^{1/2}} 2\nu \cos \frac{\omega}{2} \qquad (A.18)$$

$$\sigma_{nz} = \frac{K_I}{(2\pi r)^{1/2}} \sin \frac{\omega}{2} \cos \frac{\omega}{2} \cos \frac{3\omega}{2} \qquad (A.19)$$

$$\sigma_{nt} = \sigma_{tz} = 0 \qquad (A.20)$$

APPENDIX A5

Misprint Corrections in Ref. (20)

Two expressions derived by Kassir and Sih[20] have misprint errors which are corrected hereafter.

Eq. 46i and 46j p. 609

$$\frac{\partial^2 I}{\partial z^2} = \frac{2\xi^{1/2}[\xi(a^2b^2 - \eta\zeta) - a^2b^2(\eta + \zeta) - (a^2 + b^2)\eta\zeta]}{a^2b^2(\xi - \eta)(\xi - \zeta)(a^2 + \xi)^{1/2}(b^2 + \xi)^{1/2}} \quad b^2$$

$$\ldots - \frac{2}{ab^2}\left[E(u) - \frac{snu\ cnu}{dnu}\right] \quad (46i)$$

$$\frac{\partial^2 I}{\partial x \partial y^2} = \frac{2x\xi^{1/2}}{(\xi - \eta)(\xi - \zeta)(b^2 + \xi)^{1/2}}\Bigg/\frac{1}{(a^2 + \xi)^{1/2}}$$

$$\times\left\{\left(\frac{2y^2}{\eta - \zeta}\right)\left[\frac{\eta(a^2 + \eta)}{(\xi - \eta)^2} - \frac{\zeta(a^2 + \zeta)}{(\xi - \eta)^2}\right] - 1\right\} \quad \int$$

$$+ \frac{y^2\xi(a^2 + \xi)^{1/2}}{(\xi - \eta)(\xi - \zeta)}\left[2\left(\frac{1}{\xi - \eta} + \frac{1}{\xi - \zeta}\right)\right.$$

$$\left. + \frac{1}{a^2 + \xi} + \frac{1}{b^2 + \xi} - \frac{1}{\xi}\right]\Bigg\rangle \quad (46j)$$

APPENDIX B

NOMENCLATURE

$[C]$	original coefficient matrix
$[\bar{C}]$	reduced coefficient matrix
$[D]$	compliance tensor
$[E]$	original weighted boundary stress vector
$[\bar{E}]$	reduced weighted boundary stress vector
$E(k)$	complete elliptical integral of first kind
E	Young's modulus
G	shear modulus
I	basic elliptical integral
	$I = \frac{1}{2} \int_{\xi}^{\infty} \left[\frac{x^2}{a^2+s} + \frac{y^2}{b^2+s} + \frac{z}{s} - 1\right] \frac{ds}{[Q(s)]^{1/2}}$
K_I, K_{II}, K_{III}	stress intensity factors Mode I through Mode III
$K(k)$	complete elliptical integral of second kind
ΔK	stress intensity range
N	number of cycles
$Q(S)$	function in basic elliptical integral
	$Q(S) = S\ (a^2+s)\ (b^2+s)$
$[Q]$	matrix product $[R]^T[R]$
$[R], [\bar{R}]$	compatibility transformation matrices
$[R_s]$	boundary stress transformation matrix
$[S_k]$	coefficient matrix in Shah-Kobayashi procedure

S_{13}, S_{23}, S_{33}	components of surface stress vector, S_{33} to normal components
WELCR	special weight factor applied to the crack surfaces
T	transpose
{ }	vector
[ ]	matrix
a	crack size or major half axis of elliptical crack
a_j	coefficient in individual polynomial stress function
b	subscript for boundary or minor half axis of elliptical crack
c	constant in crack growth rate relationship
c_1, c_2, c_3	constants in harmonic stress-functions developed by Kassir-Sih
$\frac{da}{dN}$	fatigue crack growth rate
f,g,h	harmonic stress functions developed by Kassir-Sih[20] $h = C_1 . I$ $f = C_2 . I$ $g = C_3 . I$
$f_1, ---f_{10}$	harmonic stress functions developed by Shah-Kobayashi[21]
k	modulus in elliptical integrals $k^2 = 1 - \frac{b^2}{a^2}$

$\bar{k}$	complementary modulus $k^2 + k^{-2} = 1$
l_{zn}	normal to the leading edge of an elliptical crack
l_{zt}	tangent to the leading edge of an elliptical crack
n	exponent in crack growth rate relationship, total number of stress function parameters
n_f	total number of stress functions
n_s	total number of surface elements
n_R	number of reduced stress function parameters
p	constant pressure distribution on crack surfaces
$p(\bar{x},\bar{y})$	pressure polynominal according to Shah-Kobayashi[21]
$r_b(x)$	residual or boundary
$r_r(x)$	residual in region
r	subscript for region, radial distance perpendicular to leading edge of a crack
{s}	resultant stress vector transformed into the direction of the boundary stresses
s	resultant stress function, transformed into the directions of the boundary
s_i	individual stress function, transformed into the direction of the boundary stresses
snu,cnu	Jacobian elliptical functions
t	boundary stress function
{t}	boundary stress vector
$w_b(x)$	weighting function on the boundary
$w_r(x)$	weighting function in the region
x,y,z	Global coordinates

$\bar{x}, \bar{y}$	local coordinates on surface elements
α_i	stress function parameter associated with individual stress function
$'\{\alpha\}$	original stress function parameter vector
$'\{\bar{\alpha}\}$	reduced stress function parameter vector
$[\gamma]$	Shah-Kobayashi stress function parameter vector[21]
$\xi, \eta, \zeta,$	ellipsoidal coordinates where $-a^2 < \zeta \leq -b^2 \leq \eta \leq 0 \leq \xi \leq \infty$
σ	resultant stress function
σ_i	individual stress function
$'\{\sigma\}$	resultant global stress vector
$'\{\sigma_i\}$	individual global stress vector
θ	augument in parametric equation of an ellipse
ν	Poissons ratio
μ	shear modulus
ω	angle between r and l_{zn} at leading edge of a crack

VITA

The author was born in Basel, Switzerland on December 25, 1939, as the son of Mrs. M. Jaccard-Hartmann and Mr. R. Jaccard.

On October 1959 the author entered the Federal Institute of Technology, Zurich, Switzerland, where he received his diploma as a Civil Engineer in 1963.

From January 1964 to September 1965 he was a teaching assistant at the Federal Institute of Technology, Zurich with Professor F. Stussi.

In October 1965 he joined WARTMANN and Company in Brugg, Switzerland as junior engineer for the design of steel structures.

In September 1966 he became a senior engineer employed by ALUSUISSE, Zurich, Switzerland, and was in charge of the design of industrial structures in steel and concrete until April 1969. In May 1969 the author joined the staff of Fritz Laboratory, Lehigh University as a research assistant and entered the Graduate School in September 1969. As a research assistant he was associated with research on the fatigue of steel structures.